AN ABSTRACT OF THE RESEARCH PROJECT OF Robert Peckyno for the degree of Masters of Science in Geography presented on June 7th, 2010.

Title: Lava Flow Lobation and Margin Analysis

Comparative investigations based on volcanic morphology suffer from the lack of a large terrestrial baseline for comparison. To fill this gap, the Lava Flow Morphology Database (LAMDA) was proposed as a GIS based central clearinghouse for remote and field investigations of volcanic morphology. This study presents an analysis of LAMDA'S inaugural morphological feature: flow margin lobation. This study measures the margin morphology including the diameter, arc length, lobe height, cleft rate, bulbousness, and cleft angle of 1218 margin flow lobes across 30 lava flows of varied composition. While some lobe features are shown to proportionally increase as compositions become progressively more silicic, other features do not appear to correlate with compositional changes. The ultimate controlling factor behind these morphological changes is flow viscosity and calculations show an excellent correlation with lobe diameter, arc length, and lobe height, as well as a moderate correlation with flow cleft rate. The influence of local dynamics is also examined and local 'lobe level' slope, vent distance, and erosional setting are all shown to be only mildly responsible for final margin morphology. This study also examines a hierarchy of margin lobation by measuring margin lobes at multiple scales using a variety of spatial resolution data. Basaltic lava shows lobation at three spatial scales (25m ± 2, 173m ± 16, and 1027m ± 76) while rhyolites only show a single mode of lobation (435m ± 68). Finally, as an example of the utility of this dataset, it is used in three case studies: (1) to inductively compare yield strength equation predictions, (2) to calculate aspect ratios by composition, and (3) to successfully predict the composition of four 'unknown' lava flows.

© 2010 By Robert Peckyno

Defense date: June 07, 2010

All Rights Reserved.

Lava Lobation and Margin Analysis

by

Robert S. Peckyno

A RESEARCH PAPER

Submitted to

THE DEPARTMENT OF GEOSCIENCES

In partial fulfillment of the

requirements for the

degree of

MASTER OF SCIENCE

GEOGRAPHY PROGRAM

31 May 2010

Directed by

Dr. Shanaka de Silva

Acknowledgements

Thanks to everyone who helped make this project possible including: Dawn Wright, Julia Jones, Ann Nolin, Rosaly Lopes, Dave Pieri, Jack Higginbotham, Catherine Lanier, Chris Harpel, Yan Lavalee, Jeff Burns, Chuck Wood, Axel Schmitt, Ted Harbaugh, David Hume as well as the Cascades Volcano Association, the Tower Geosciences Grant, the Oregon Space Grant Consortium, the ASTER Science Team, the NASA Jet Propulsion Laboratory, ESRI, Google Earth and the Dharma Initiative.

Special thanks to Shan beyond calculation for direction, assistance, honesty, adventure, and friendship. Your impact extends far beyond academics and I can't begin to thank you for all the good that has come from it.

Laura, I promise this is my last degree…. really… probably… Thanks for putting up with all this nonsense!

Table of Contents

Table of Figures

A COMPARATIVE ANALYSIS OF LAVA FLOW MARGIN LOBATION

Abstract

Comparative investigations based on volcanic morphology suffer from the lack of a large terrestrial baseline for comparison. To fill this gap, the Lava Flow Morphology Database (LAMDA) was proposed as a GIS based central clearinghouse for remote and field investigations of volcanic morphology. This study presents an analysis of LAMDA'S inaugural morphological feature: flow margin lobation. This study measures the margin morphology including the diameter, arc length, lobe height, cleft rate, bulbousness, and cleft angle of 1218 margin flow lobes across 30 lava flows of varied composition. While some lobe features are shown to proportionally increase as compositions become progressively more silicic, other features do not appear to correlate with compositional changes. The ultimate controlling factor behind these morphological changes is flow viscosity and calculations show an excellent correlation with lobe diameter, arc length, and lobe height, as well as a moderate correlation with flow cleft rate. The influence of local dynamics is also examined and local 'lobe level' slope, vent distance, and erosional setting are all shown to be only mildly responsible for final margin morphology. This study also examines a hierarchy of margin lobation by measuring margin lobes at multiple scales using a variety of spatial resolution data. Basaltic lava shows lobation at three spatial scales (25m ± 2, 173m ± 16, and 1027m ± 76) while rhyolites only show a single mode of lobation (435m ± 68). Finally, as an example of the utility of this dataset, it is used in three case studies: (1) to inductively compare yield strength equation predictions, (2) to calculate aspect ratios by composition, and (3) to successfully predict the composition of four 'unknown' lava flows.

Introduction

As lava flows across the landscape and cools, the final shape and surface morphology that it will develop is related to the intrinsic properties of the eruptive material (composition, rheology, etc.) and the extrinsic forces acting upon it (friction, gravity, slope, etc.). (e.g. Rossi, 1996; Fink and Griffith, 1998; Griffith, 2000; Gregg and Smith, 2003) On Earth, lava flows can be studied at length by armies of scientists in the field and followed by detailed chemical analyses' and laboratory techniques that can be applied to uncover at least some of the materials history. But, lava flows have been imaged on several other solar system bodies including: Mercury (e.g. Head, et.al, 2009), Venus (e.g. Head, et.al, 1992), the Moon (e.g. Hulme and Fielder, 1977), Mars (e.g. Theilig and Greeley, 1986; Wadge and Lopes, 1991), Io (Williams, et.al, 2001), and Titan (Lopes, et.al. 2007) and humans simply do not have the infrastructure in place to undertake solar system field geology. Even surface analysis by robots is prevented by the complex and broken terrain of lava flows (Curtis et al., 2006) and the associated increase in mission difficulty, complexity, and cost (Lopes, 1993). Consequently, a majority of the information currently known about extraterrestrial lavas has been obtained through the interpretation of remotely imaged flow features and spectroscopic data and by using models to relate final flow morphology to eruption rate, magma chemistry, and tectonic mechanisms (Griffiths, 2000).

This methodology has been quite successful and there are multitudes of comparative morphology studies (e.g. Carr and Greeley, 1980, Wadge and Lopes, 1991, Burns, 2002, Baloga, 2003, many others). Through field analysis and laboratory simulations, numerous factors have been identified that influence the final morphology of a lava flow including overpressure,

eruption rate/volume, lava rheology and yield strength, ambient temperature, and ground slope. (e.g. Rossi, 1996; Wadge and Lopes, 1991; Bruno, 1994; Fink and Griffith, 1998; Stasiuk and Jaupart, 2002; Gregg and Smith, 2003; Gregg and Keszthelyi, 2004). These studies have all shown a clear morphological and compositional progression ranging from low profile basalts to steep rhyolitic domes. However, data availability and computing power have limited prior studies to comparisons between a small subset of lava flows and/or features. Consequently, no terrestrial 'baseline' of existing lava flow morphology has been established.

Modern satellite imaging and topographic data products are approaching the spatial resolution necessary to inductively explore lava flow morphology and modern computing power has enabled doing so on a planetary scale. That is the goal of the Lava Flow Morphology Database (LAMDA) (Peckyno and de Silva, 2009; Peckyno et.al, 2009) and this research takes the first steps towards that goal focusing on the lobation and morphology of lava flow margins. The goals of this analysis are twofold. First, quantifying the size and shape of these morphological 'steps' on a large representative dataset will provide an improved baseline against which remote flow compositions can be inferred. Second, this dataset provides bulk real-world data to inductively examine existing lava flow models.

Advancement and Justification

Spatial resolution has been a common limiting factor in prior planetary analog studies. Lava flow margin lobes can vary in width from a few meters to over a kilometer from cleft to cleft. In basaltic lavas, these margin lobes are often fractal in nature (Bruno, 1994). The

implications of this in remote sensing studies is that large lobate flows appear to have smooth margins in low resolution data while, in reality, they are divisible into smaller flow lobes beyond the limits of the resolution (e.g. Burns, 2002). Lopes and Kilburn (1990) also warned that the vertical resolution of available extraterrestrial slope data was likely too low for detailed flow analysis. Using Viking 50-m spatial resolution data, Wadge and Lopes (1991) analyzed the flow lobes of Olympus Mons, but this data would be insufficient to see the smallest scale of basaltic lava flow lobes. They stressed that the analysis of extraterrestrial lava flows is primarily hampered by our ignorance of terrestrial lavas and the lack of a large morphological dataset for comparison.

Since that time, significantly higher spatial and vertical resolution data has become available for both Earth and Mars. On Earth, 1m imagery of nearly everywhere on the planet is widely available and high resolution topographic products are starting being produced. Mars has also been placed under the high resolution microscope. The Mars Global Surveyor, carrying the Mars Orbiter Laser Altimeter (MOLA), has a topographic vertical resolution under 5m, and the Mars Reconnaissance Orbiter, carrying the High Resolution Imaging Science Experiment (HiRISE), has a spatial resolution of less than 1m. This study took advantage of these and other new high resolution datasets to holistically investigate and measure the margin lobation of thirty (30) lava flows. These measurements provide the foundational dataset for the Lava Morphology Database (LAMDA), a statistically based cornerstone for extraterrestrial volcanic flow investigations. In addition to the scientific interest, this is also socially relevant as managing the hazards of lava flows depends on modeling the ways in which lava will flow across a landscape, how it will respond to topography, and the ultimate distance it will travel before coming to rest.

This dataset enables a deeper investigation into whether intrinsic fluid properties or extrinsic spatial and topographic variation are the primary controllers of flow margin morphology.

This study also differs from prior studies in two primary ways. First, prior margin lobation studies (e.g. W&L, 1990) have focused primarily on the distal lobes of flows. By contrast, this study measures margin lobation irrespective of distance from the vent or spatial relationship to the channel. Secondly, while the ground slope of the underlying topography is considered one of the most important factors that influence the direction and morphology of a flow, (Gregg and Fink, 2000) data resolution and computing power have often necessitated that researchers assume that local slopes, viscosities, chemistries, and temperatures are constant across a flow. In contrast, this study examines the emplacement of lava flows at a much higher resolution than previous studies by extracting the local slope underneath each individual flow lobe rather than using a constant slope value across the entire lava flow.

Methodology

A majority of the measurements taken for this analysis were performed in ArcGIS across multiple satellite image datasets including: the Moderate Resolution Imaging Spectroradiometer (MODIS), The Landsat Missions, the Advanced Spaceborne Thermal Emission and Reflection Radiometer (ASTER), and other higher resolution satellite data and aerial photography as available for each of the lava flows. Additionally, multiple elevation datasets (e.g. the Shuttle Radar Topography Mission (SRTM) Digital Elevation Models (DEMs), ASTER relative DEMs, the USGS Oregon 10m dataset, etc.) were obtained for all lava flows. Compositional maps, if available, or other relevant datasets were imported, rectified as needed to the best resolution

imagery, and projected into an appropriate cartographic projection for the region in question. All calculations were done using measurements taken from the highest resolution dataset available for the lava flow in question. Morphological features were measured on thirty (30) lava flows across the compositional spectrum and erosional environments. Selection for this dataset mimicked much of the Wadge and Lopes, 1991 dataset, with the addition of multiple Chilean and Oregonian lava flows that were measured during the proof of concept phase of this study. These additions enabled a comparison of lobe morphologies in different climates and erosional environments as well as three field ground truth studies to constrain error margins [See Appendix 1 for a complete listing of flows measured for this study].

Margin lobes were chosen as the foundational dataset for LAMDA because they are easily measurable in remotely sensed images, they show differing levels of detail at varying resolutions, and they have been explored at length in the field and in the laboratory in relation to process. Flow lobe features that were analyzed for this study were lobation radii, cleft to cleft distance (arc length), and intercleft (or reentrant) angle. [Figure 1] Lobe bulbousness, aspect ratios, nearest neighbor distances, and cleft rates were also calculated from those values. Underlying local slope values were interpolated from the DEM. All flows were reprojected into an appropriate equal area local projection and datum before measurements were taken. Measured values were subsequently plugged into two relevant fluid models (Hulme 1974, Blake 1990) and compared with field derived yield strength and compositional values. All flow compositional values were obtained from the literature and samples were not reanalyzed for this study.

Figure 1: Lobe features measured for this study

Margin Lobation

Why Lobes?

One common way of describing the movement of a lava flow is via the Bingham fluid model. (Shaw et al 1968; Murase & McBirney 1973; Hulme, 1974; etc.) In this model, lava flows down a slope (θ) driven by gravity (g) with the lateral component of flow being governed by the lava's yield strength ($\boldsymbol{\tau}$). In order for lava (or any material) to flow, a stress that is greater than its yield strength must be applied. This is the shear stress at the base of the flow created from the weight of the material. At the central point of a lava flow channel this relationship can been described as:

$$\boldsymbol{\tau = g\,\rho\,h\,sin(\theta)} \qquad \textbf{(1)}$$

where ρ is the density of the lava and *h* is the depth in the center of the channel. Near the edges of the flow, depth decreases and lateral flow stops when the sheer stress pressure is balanced by the flows yield strength. The equilibrium state can hence be related to the height of the lobe (H) and the radius of the lava lobe (R) (Blake, 1990, Wadge and Lopes, 1991) as:

$$\tau \sim g\rho H2/R \qquad (2)$$

Building on this model, Wadge & Lopes (1991) proposed that the widths of the distal lobes of lava flows are representative of the arrest of free-flowing isothermal Bingham fluids on a slope and hence the rheology of the lava. By measuring lava flow lobe widths in remotely sensed data and comparing them with field analysis data, they found a positive correlation between the silica content of the lava and the width of 465 distal flow lobes.

Modern high spatial resolution remotely sensed data reveals what is obvious in the field, that lava flows form small margin lobes nearly everywhere that a flow cools and stops without a barrier or restriction, not just at the distal end of a flow. This study builds upon their findings measuring 1218 flow margin lobes across the margins of 30 flows and correlating them with distance from source, underlying lobe level local slope, silica compositions and calculated viscosities. Further, this study examines several related additional margin properties and features including cleft rate, arc length, lobe height, cleft angle, aspect ratio and lobe bulbousness [Figure 1]. The physical basis for each of these features, the methodology used to take the measurements, and basic composition based analysis follows.

Methodology and Measurements

Lobe Diameter

Using the ArcGIS drawing tools, circular shapefiles were created for each lobe along the margin of each lava flows. Lobes were defined as any bulbous area extending beyond the

straight line margin of a lava flow. Cleft angles on both sides of the lobe were required to be <135 degrees to be considered an independent lobe except in circumstances where the entire flow terminated in a single lobe. Shapefiles were expanded by hand until the maximum amount of the lobe margin lay along the circumference of the circle [Figure 2]. Area, circumference, radii, and elevation differentials were calculated for these circles in ArcGIS and the results were exported to Microsoft Excel and plotted versus composition [Figure 3], lobe level local slope [Figure 15], and distance from the vent [Figure 19].

While hand drawing shapefiles does introduce a margin of the possibility of a few meters variability due to human perception error, it is minor in comparison to the dramatic changes in lobe size due to composition. Flows were categorized according to lava composition into the following bins in Table 1. Smaller confidence intervals reflect the far greater rate of lobation (and consequently n-values) for basaltic lava.

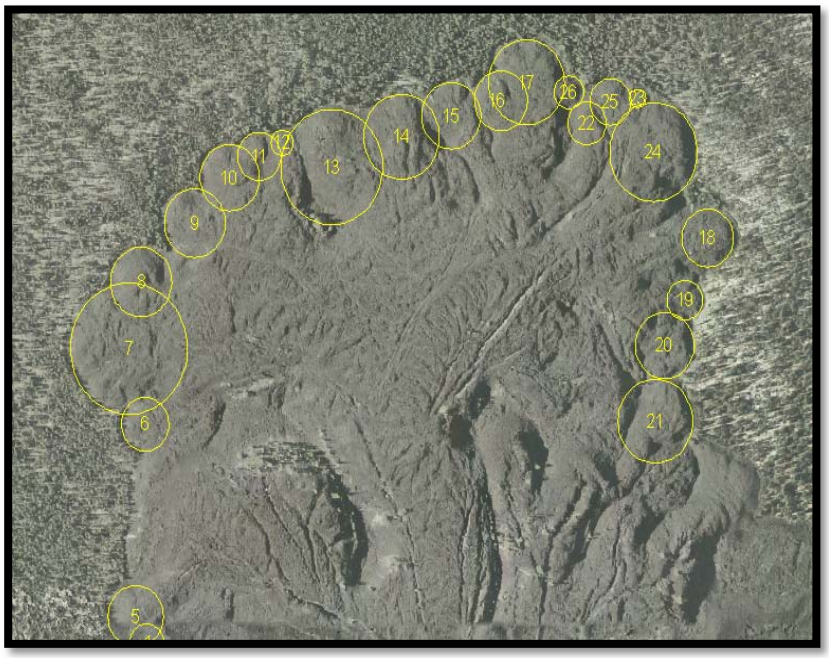

Figure 2: Circular shapefiles over margin lobes at Black Rock lava flow, Oregon

Table 1: Mean lobe widths by composition

Category	Silica Composition	N (Lobes measured)*	Mean lobe width (m)	95% (ci) confidence interval
Basalt	45-52%	333	26m	±2m
Basaltic-Andesites	52-58%	484	49m	±3m
Andesites	59-64%	348	152m	±9m
Dacites	64-72%	42	518m (w/Chao) 409m (wo/Chao)	±104m
Rhyolites	72+%	11	539m	±149m

* See Appendix A for a complete listing of flows.

Plotting radii versus composition [Figure 3] confirms the linear relationship between lobe size and composition first uncovered by Wadge and Lopes (1991). However, these results build upon their findings by showing that the diameter of the smallest visible lobes remains relatively consistent across a lava flow irrespective of distance from the vent or positional slope. Tube fed lobes at the distal end of a flow, show little morphological difference to lobes that formed proximal to the vent before channelized flow developed. This strongly suggests that while eruption rate may alter the length and overall size of a flow field, the margins have disconnected from the eruptive regime and their final morphology results only from a combination of fluid rheology and underlying ground slope.

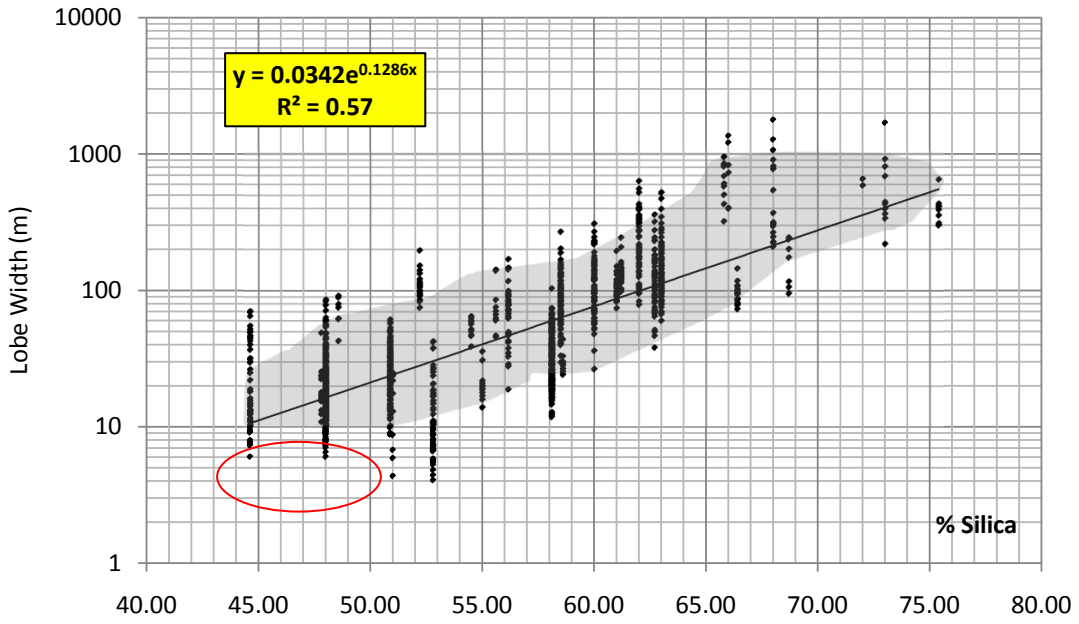

Figure 3: Lobe Diameter vs. Silica Content (All Lobes) / Cloud represents Wadge and Lopes, 1991 results.
Resolution data hole (discussed below) noted in red.

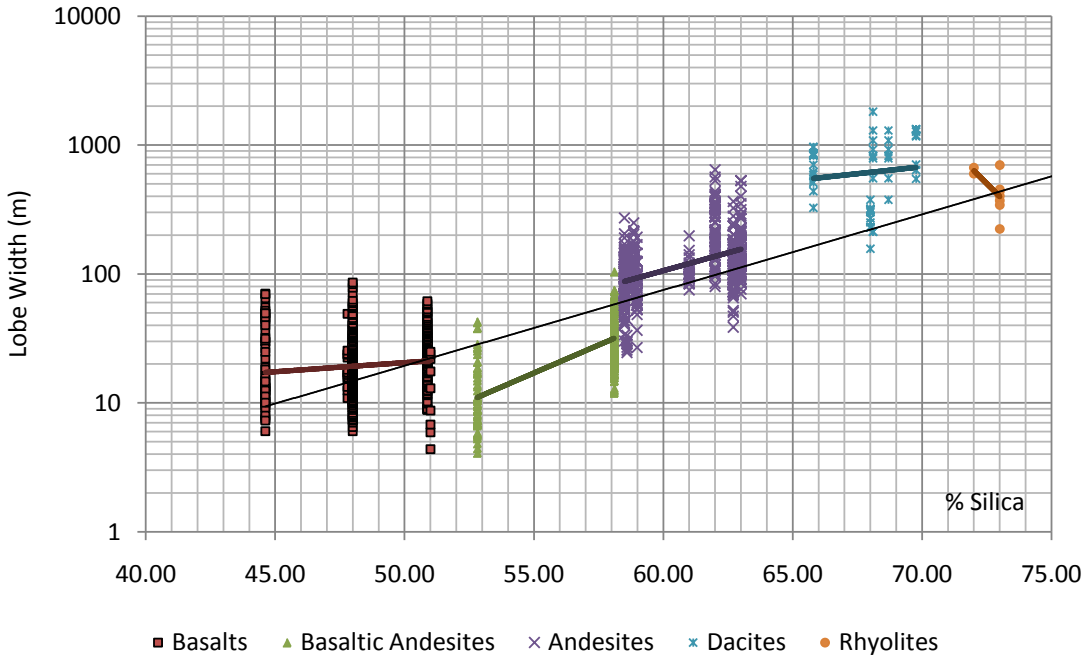

Figure 4: Lobe Diameter vs. Silica Content (by Composition)

(Overall trend shown in black, compositional trends shown as colored dashed lines.)

As noted in Figure 3, there is a hole in the data of lobes beneath smaller than 10m. Even in high resolution data, lobe measurements are very imprecise below 10m and potential errors due to operator perception and data map reprojection make these measurements unreliable. However, in basaltic lava, it is the 1-10m lobes that record the local advance of a flow (Gregg and Keszthelyi, 2004) and these lobes are simply too indistinct and too small to be precisely measured with satellite resolution data. Only aerial and field based LIDAR sensors are capable of clearly seeing 1m lobes with sufficient (.3m) accuracy (Vilardo and Ventura, 2004). That resolution would enable the remote analysis of very low viscosity flows like Etna, Kilauea, and Vesuvius, which of course, would alter our slope. [Figure 5]

Figure 5: Kilauean Lava Lobes – 10m lobe marked

Based on the range and variety of 1-10m margin lobes found in the field at Kilauea [Zimbelman et.al, 2008], 100 hypothetical random additional flow lobes representing Etna, Kilauea, and Vesuvius (or other similar low viscosity lavas) were added to ascertain their effect on the model slope. The addition of these hypothetical lobes further improves the model. [Figure 6]

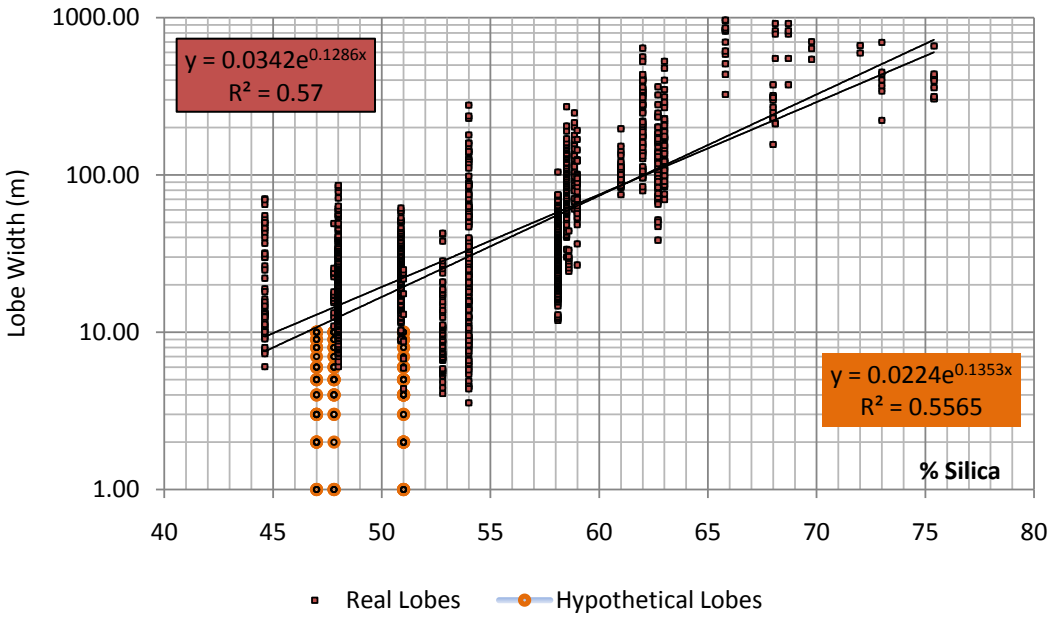

Figure 6: Width vs. Composition including hypothetical Basaltic additional lobes. (orange)

Cleft to Cleft Distance (Arc Length)

Any fluid system that moves at a nearly constant velocity normal to the front will develop clefts (McElwaine & Patterson, 2004). In laboratory experiments, Simpson (1974) showed that by moving the floor in the direction of the current, the formation of lobes and clefts could be completely suppressed concluding that fluid cause for the development of lobes and clefts along the front of a gravity current is the influence of the underlying ground at the leading edge of the flow (Simpson, 1997).

Using lava analogs, the evolution of these instabilities have been studied at length in the laboratory (e.g., Simpson, 1997; Griffiths and Fink, 1992; Fink and Griffiths, 1998; Gregg and Fink, 2000; Hartel et al., 2000; Blake and Bruno, 2000). It has been found that there is a maximum possible lobe size before a new cleft will form. Further, while these lobes and clefts

are constantly being created, moving and merging with each other as the flow progresses downslope, the number and size of the lobes and clefts has been shown to remain relatively constant (Simpson, 1997; McElwaine and Patterson, 2004).

Figure 7: Arc lengths or 'cleft to cleft' distance

For this study, arc length is defined as the cleft to cleft distance measured along the flow lobe margin. Linear shapefiles were manually drawn from cleft to cleft in ArcGIS as shown in Figure 7 and distances were calculated. As arc length and lobation radii are connected, it is not surprising that arc length distances also increase along the same linear trend with composition. [Figure 8]

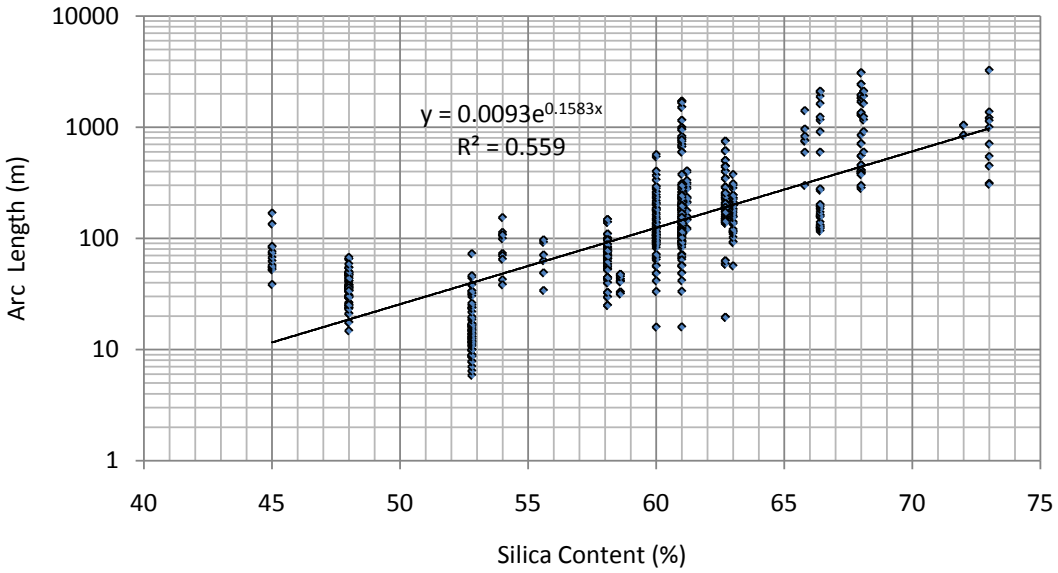

Figure 8: Arc length vs. SiO_2

Bulbousness

While the arc length distances remain relatively consistent with respect to composition, there is a large variety in the amount that the lobe protrudes from the flow perimeter. This can be seen in Figure 9 where the four highlighted arc lengths are of identical length, but clearly not of identical shape. To explore the causes behind this variety, this study creates a 'bulbousness' term defined as the percentage of the flow lobe that is actually on the margin of the flow. This value was derived by taking the full circumference of the lobe circle and dividing by the arc length or cleft to cleft distance.

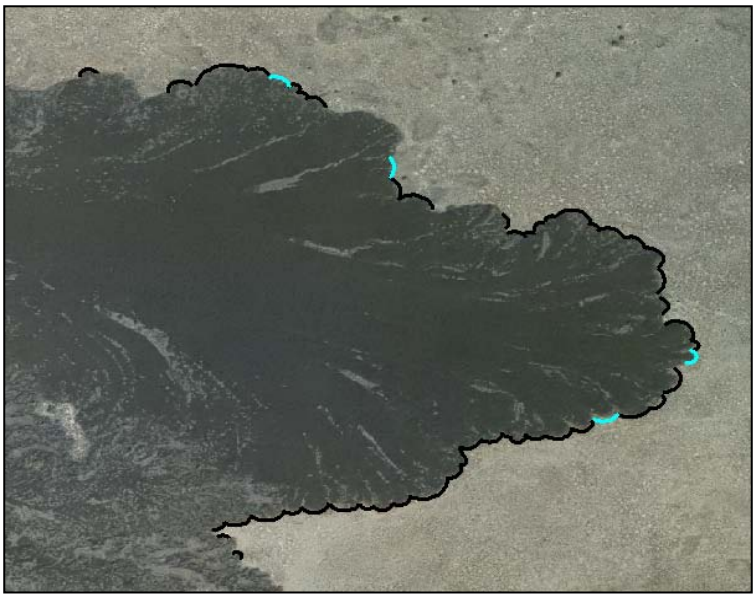

Figure 9: Four equal arc lengths at Four Craters lava flow, Oregon

However, no correlation was found between composition and lobe bulbousness (Figure 10) or local slope.

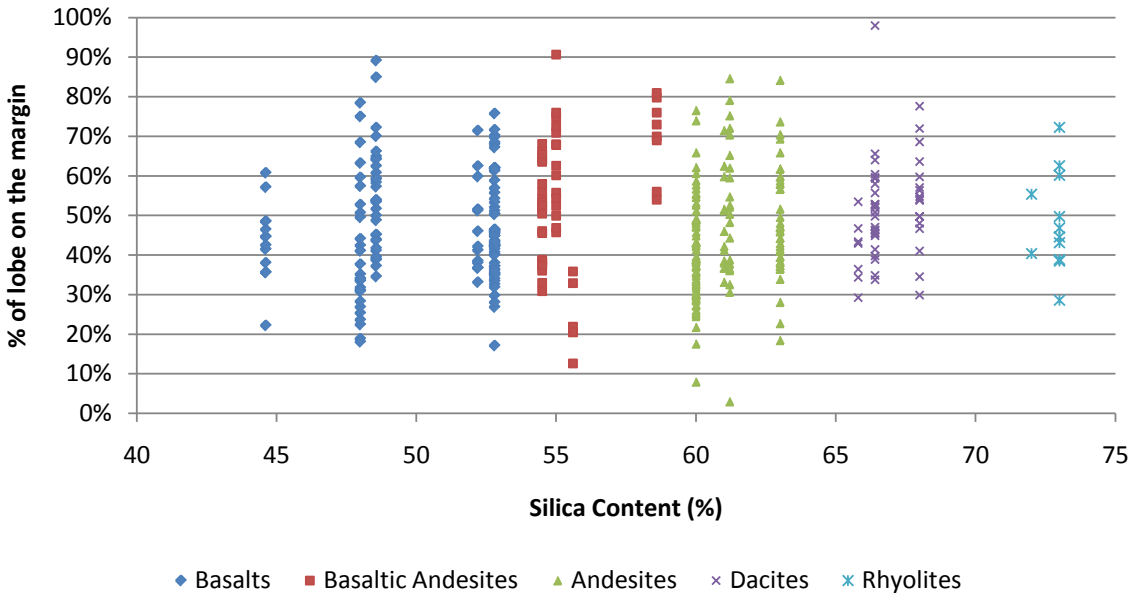

Figure 10: Bulbousness versus Composition

Intercleft Angles

Intercleft angles are defined as the angle between two adjacent lobes. As stated previously, for a lobe to be considered, the angle on both sides of the lobe needed to exceed 135 degrees. This value was chosen because it mirrors the Wadge and Lopes, 1991 criteria.

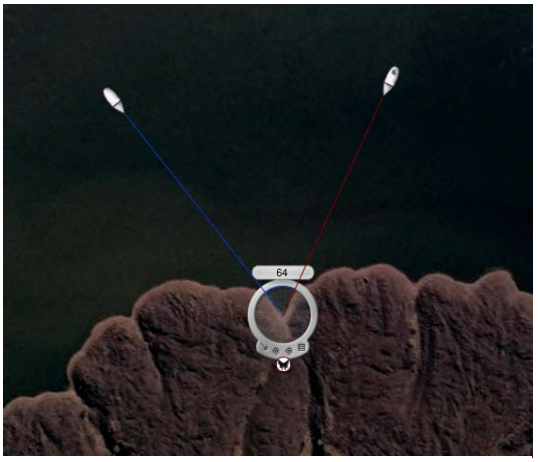

Figure 11: Intercleft angle measurements at Davis Lake lava flow, Oregon

Angles were manually measured using a digital protractor and correlated with the lobes that flanked it as seen in Figure 11. Intercleft angles were highly variable irrespective of composition and are shown in Figure 12.

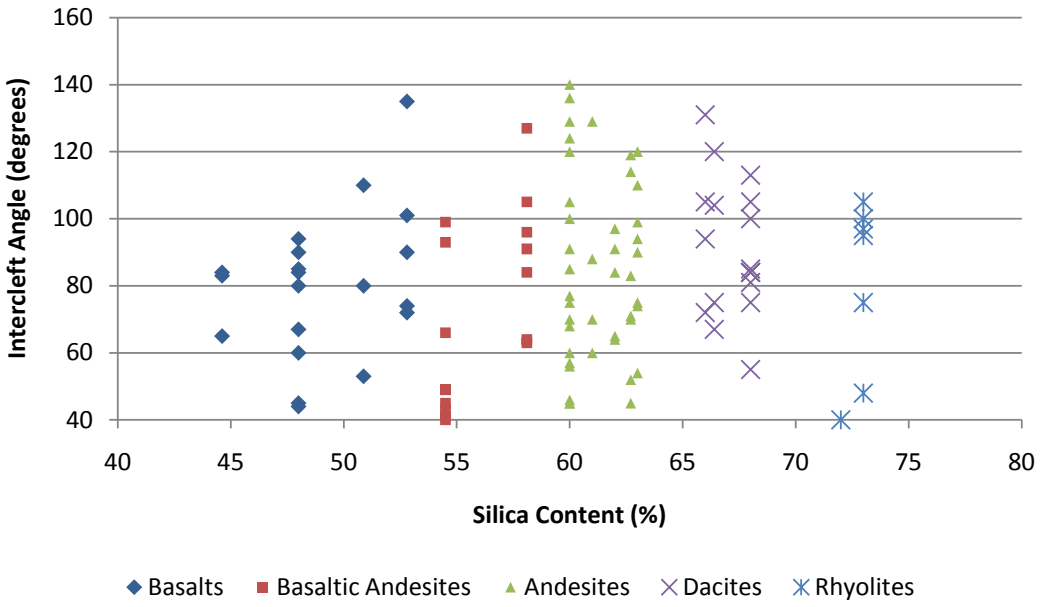

Figure 12: Intercleft Angle vs. Composition

Intercleft angles were also plotted against lobe size to explore possible correlations. However, there appears to be no impact of variable lobe size on intercleft angles. (Figure 13)

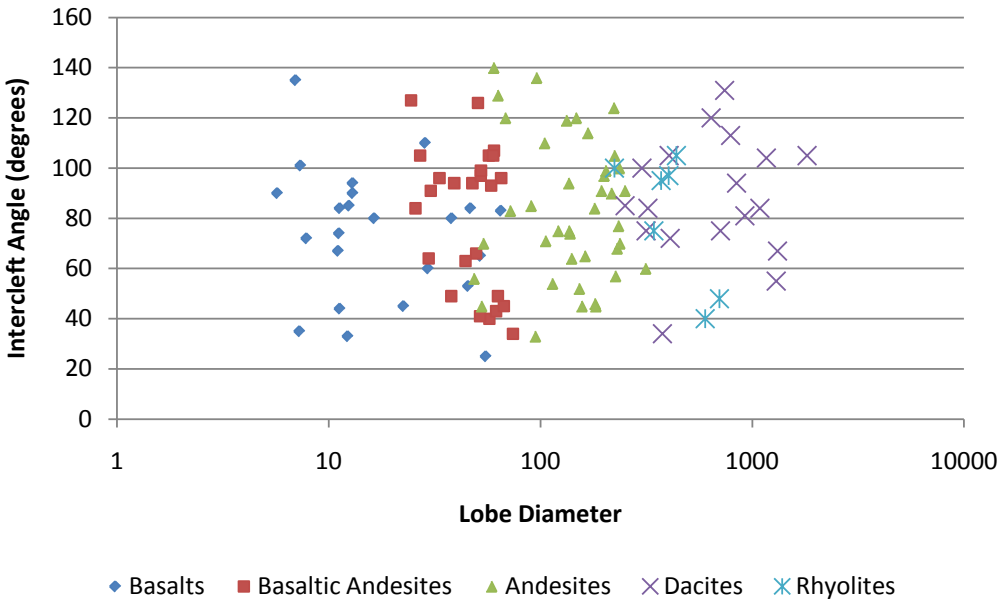

Figure 13: Lobe Diameter vs. Cleft Angle

Lobe Level Slope/Aspect

A majority of elevation data was extracted from the ASTER Global DEM, but as Table 1 showed, the mean size of basaltic lobes is beneath the 30m resolution of the ASTER Global DEM. For all Oregon lava flows, 10m resolution DEM's followed by field ground truth was used to calculate lobe heights and local slopes. The elevations of the end and center points of the arc were extracted from the DEM and a Triangulated Irregular Network (TIN) model was created from these point sets. [Figure 14]

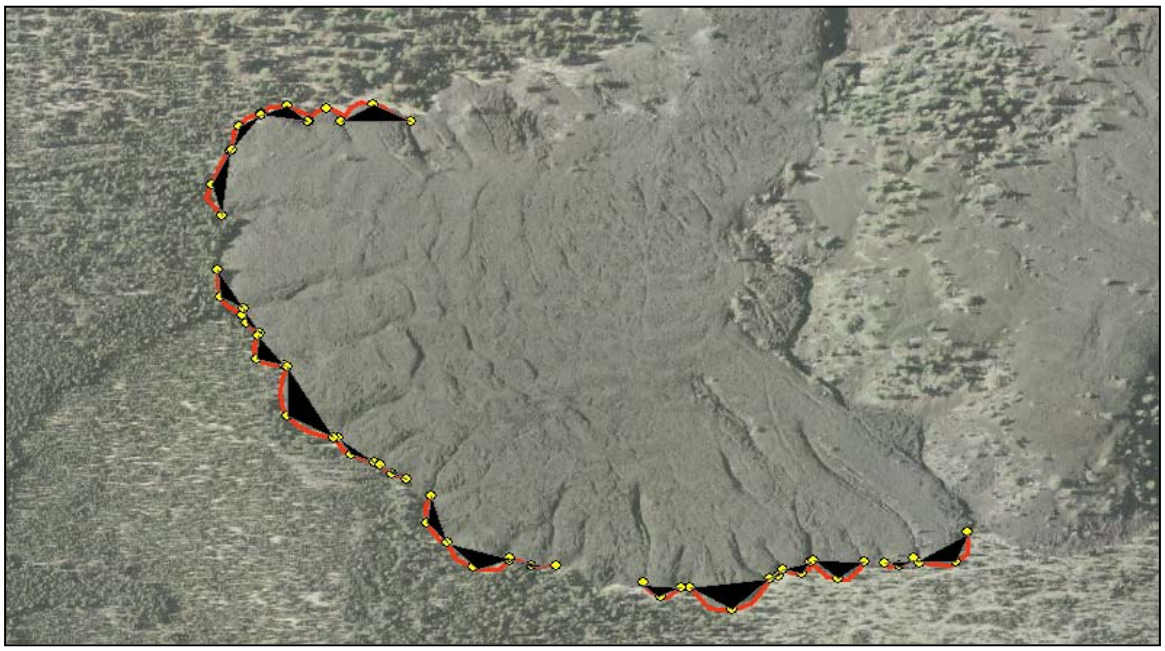

Figure 14: Yellow points represent the ends and center of the arc.

TIN slopes and aspects were then generated.

These values give a reasonable approximation of the slope and aspect of the underlying topography at the lobe level. Viewed across the entire dataset, this method enables a direct comparison of lava flow lobe size and arc length to underlying slope. The following figures both eliminate very large lobes (greater than 1km for data visibility, however it should be noted that the largest, higher silica, flow lobes were all on slopes of less than 20 degrees.

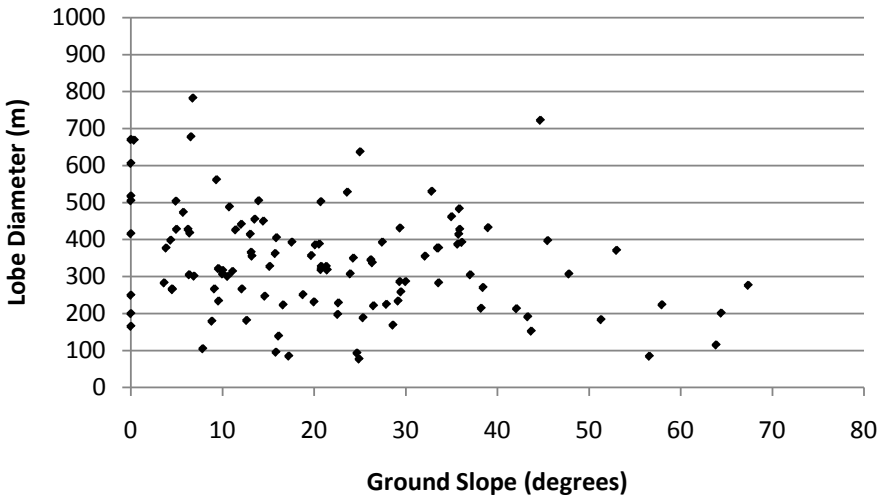

Figure 15: Lobe diameter v. Local Slope

While the number of lobes decreases at higher slopes, Figure 15 shows lobes smaller than 800km are common on ground slopes up to 40 degrees suggesting that local changes in slope may only be a minor component in the final size of a margin lobe. Arc length [Figure 16] plots mirror this showing arcs of less than 300m are common across through 40 degrees and drop off as slope increases.

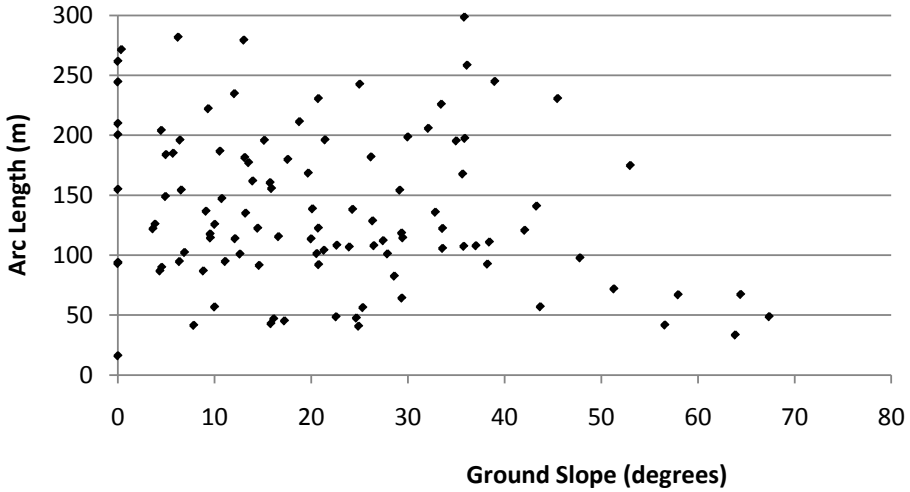

Figure 16: Arc Length v Local Slope

Lobe level aspects were also generated and compared against the flow direction to look for topographically driven changes in lobe size and flow direction. For instance, in Figure 17, the TIN aspect showed lobes two and five were flowing 'uphill' which plausibly explains (due to ramping against topography) why the resultant lobes are wider and thicker.

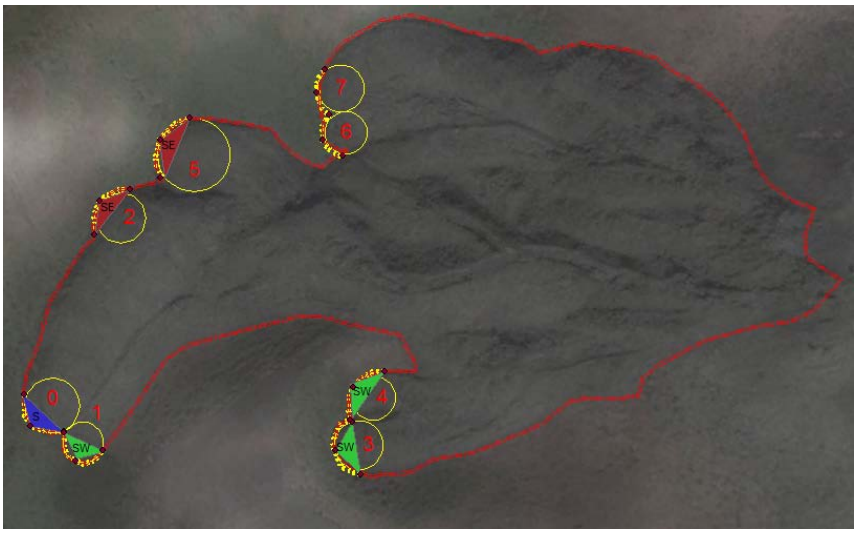

Figure 17: TIN Aspects compared with flow direction at Akita lava flow

Flow Spread and Distance

Vent locations were marked with a point shapefile and axial diagrams were made from that point to the perimeter of the lobes on the margin to measure the lobe distance from the vent. An example of this process is shown in Figure 18. These values were then plotted against lobe size and show that lobes of all sizes can occur across a wide range of distances. Categorized by composition, the data shows no correlation between lobes size and source distance. [Figure 19]

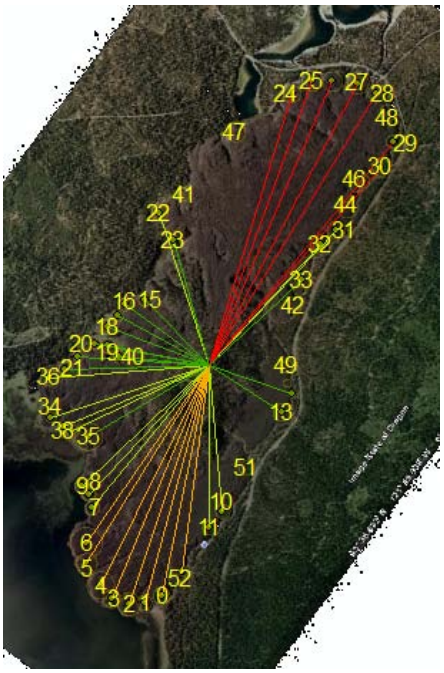

Figure 18: Axial Diagram of Davis Lake lava flow

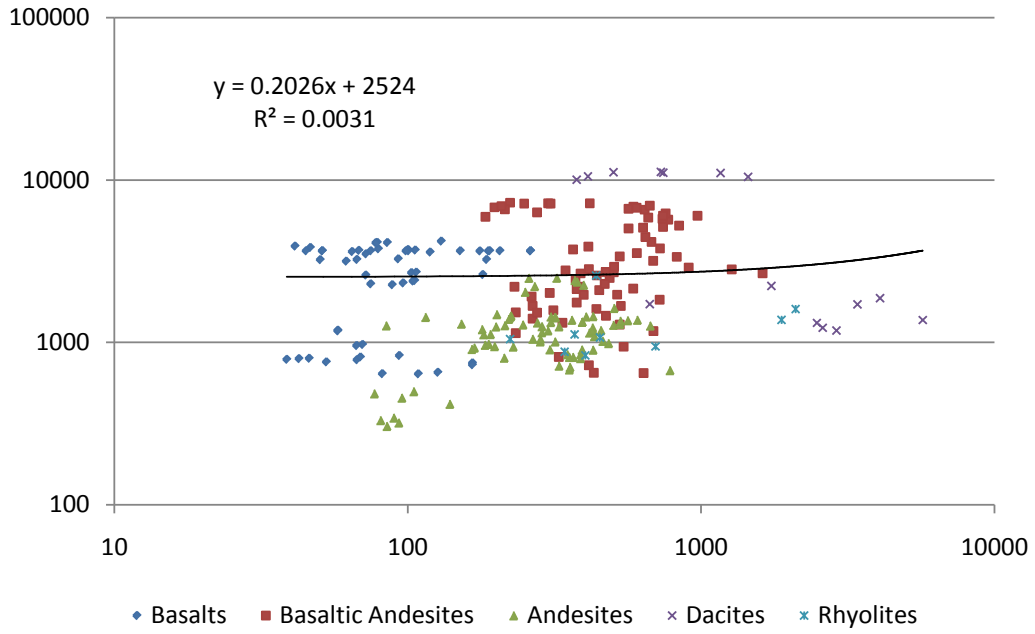

Figure 19: Distance from Source vs. Lobe Size

While these conclusions may naturally be biased by the large number of lobes that form in basaltic lava, these results suggest that final margin morphology is primarily controlled by lava rheology and not the distance from the vent.

Lobe Height

Lobe height, for this analysis, was calculated by subtracting the elevations of the two end and the central point of the arc length shapefiles from the elevation of the centroid of the lobe circular shapefiles, the theoretical 'center' of the lobe, to generate a max/min possible height

value. Height values were plotted versus composition [Figure 20], local slope [Figure 21], and width values for aspect ratio calculations. [Figure 34]

The height of the smallest visible lobes increased through dacitic compositions maxing out with the ½ km tall lobes at Chao. Basaltic lobe heights were rarely above the 30m ASTER Global DEM vertical resolution and often not even clearly visible in the 10m Oregon State DEM. Only LIDAR would be capable of performing this analysis on basaltic flows, but very little data is currently available for remote areas of purely geologic interest. However, basaltic data correlated well with the trend established by more silicic lava as seen in Figure 18 and provide an effective way to differentiate between large basaltic lobes from similar sized silicic lobes.

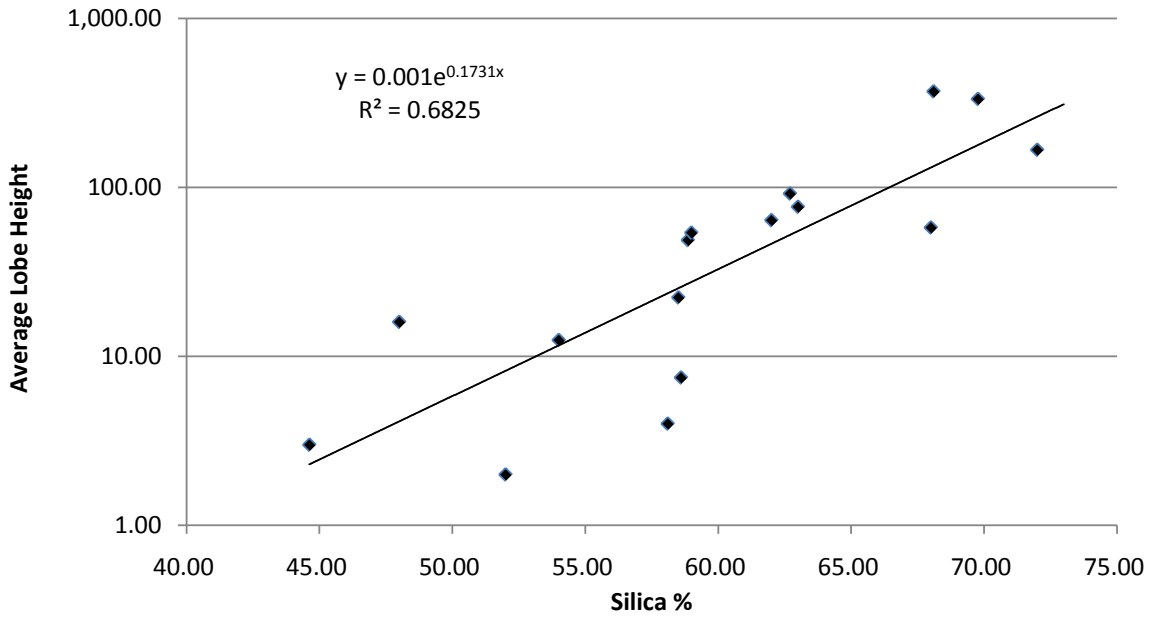

Figure 20: Average Lobe Height versus Composition

Calculated height values were also plotted versus the locally derived slope values and show essentially no correlation. [Figure 21] However, the high slope values calculated using the methodology above, may not be reflective of reality as they may be based on changes in topography that are either so small that the values become noise or due to registration errors.

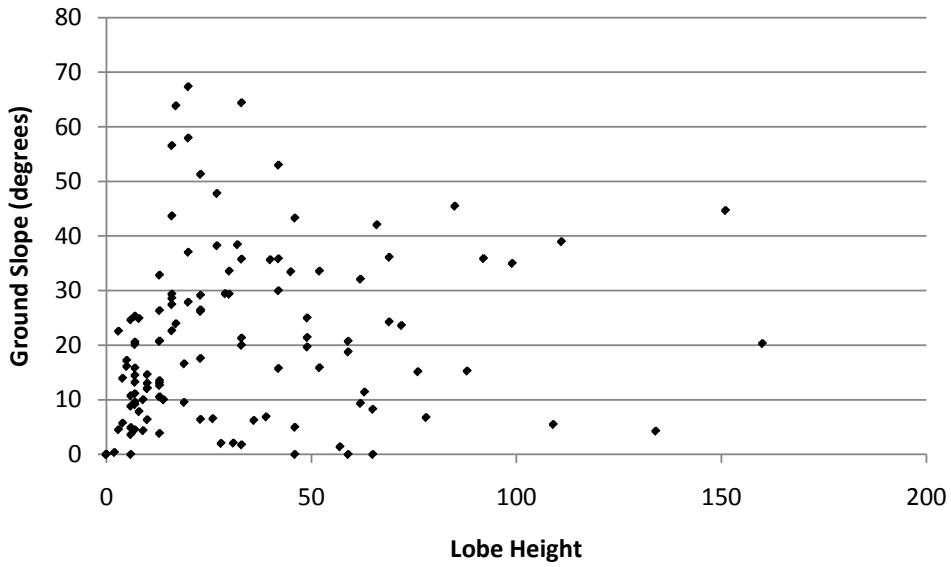

Figure 21: Lobe Height vs. Local Slope

Lobation Density and Cleft Rate

The 'rate of lobation' is defined as the number of clefts per unit distance. To determine these values, point files were created for each cleft point along the outline of the flow. (Figure 22) This was primarily used to uncover sites of interest rather than for actual data. To

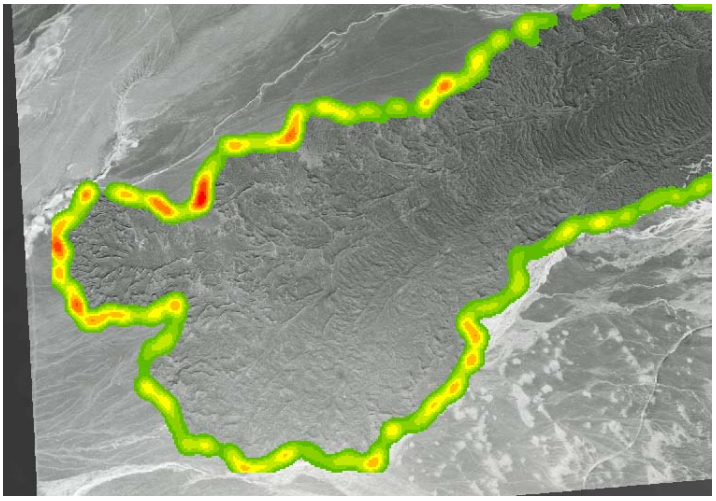

Figure 22: Density of lobation

ensure that the highest resolution clefts were being counted, Google Earth (~1m) imagery was used to determine cleft rates. Multiple manual counts of lobe clefts along random 1km transects were averaged. Basaltic lobes averaged 15 clefts/km and had as many as 30 clefts/km. Considering the fractal nature of basaltic flow lobes (Bruno, et al., 1994) this can likely be further subdivided all the way to fingerling breakouts on the cm scale. As the compositions evolved through rhyolites, there were progressively less clefts as seen in Figure 23.

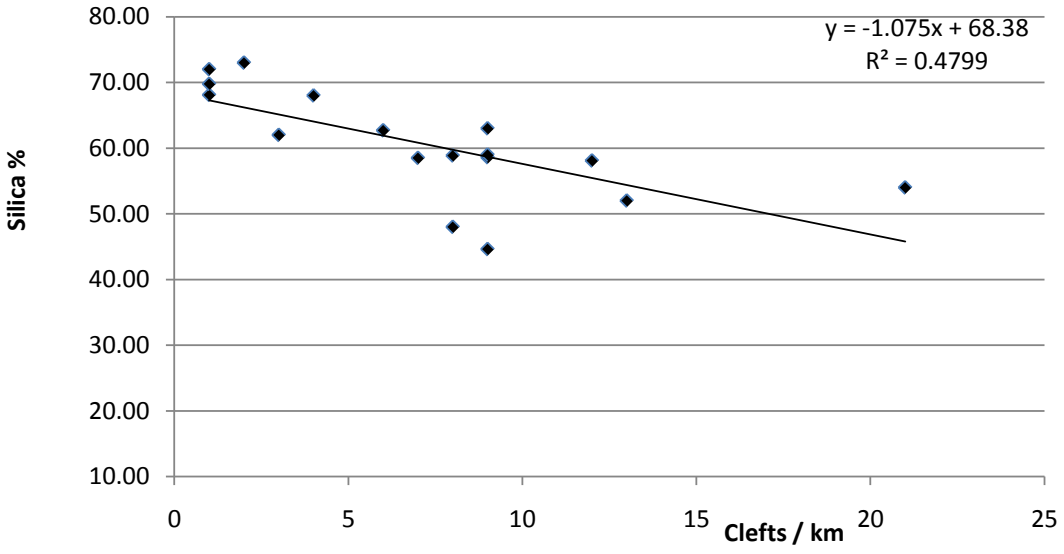

Figure 23: Average clefts / km v. Silica

Nearest Neighbor Analysis

Once the centroids of each lobe were calculated, a nearest neighbor analysis was performed finding the average distance from one lobe center to the next closest lobes center. [Figure 24] The distance from one lobe to the next increased consistently as composition increased. However, there would be a natural increase in distance due to the size and scale of the lobe themselves. Averages for flows show that less viscous lava is affected to a greater

extent by resistance and friction from the underlying ground (the cause of cleft formation - Simpson, 1974) consequently forming significantly greater numbers of clefts ultimately responsible for a greater density of flow margin lobes.

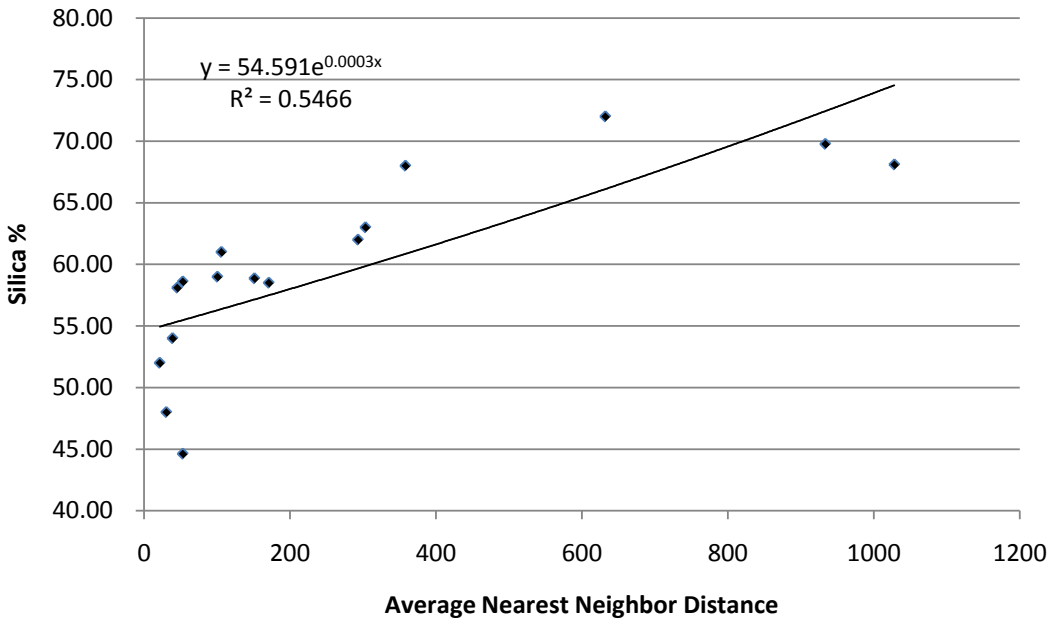

Figure 24: Average nearest neighbor distance v. silica content

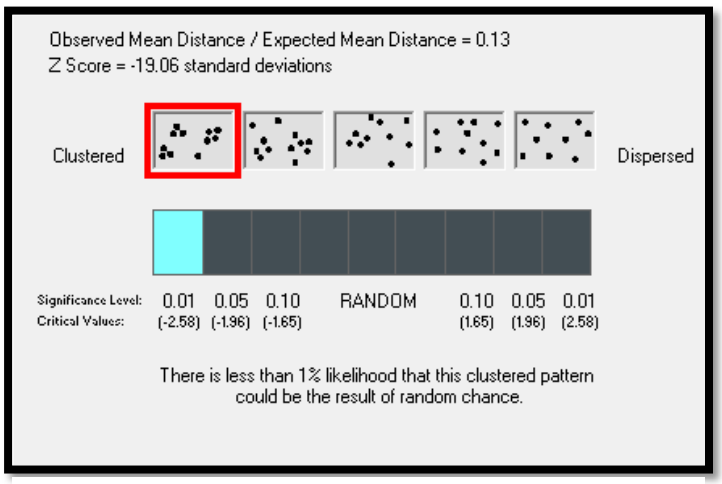

Figure 25: Average Nearest Neighbor Summary for Lava Butte lava flow –> Observed Mean Distance = 39.45m

Observed mean nearest neighbor distances were determined for each flow in Arc. Spatial analysis tools (Figure 25) also gave some insight into the spread of the lobes at a flow and pair well with the density of lobation diagrams discussed earlier.

Hierarchy of Lobation Analysis

The systematic creation of lobes along a flow creates a diagnostic margin crenulation that can be directly related to the fractal dimension of the lava flow. Bruno, et al., (1994) used this relationship to discriminate between a'a and pahoehoe lavas. Welhan et al., (2002) further explored this concept using a modified nearest neighbor quadrant analysis of the Snake River lavas in Idaho. Margin lobes also show a degree of fractality that was uncovered while exploring the importance of data resolution on this type of morphology analysis.

As we've already seen, the size and scale of lobes vary with composition. However, they also vary with the spatial resolution of the satellite data currently under analysis. Lower resolution spatial data (such as the MODIS and LANDSAT images of North Sister (OR) lava flow above) gave insight into the broader levels of lobation occurring across a flow while high resolution spatial data enabled a high resolution exploration of even the smallest of flow margin lobes.

Table 2: Three levels of lobation resolution at North Sister, Oregon

		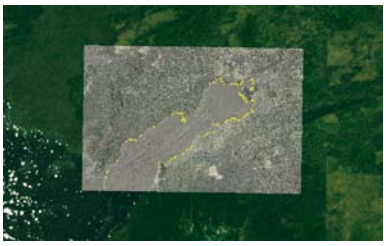
A higher order lobe from North Sister shown at MODIS resolution	The same flow lobe at LANDSAT 30m resolution. Margins lobes on a second are visible (some noted in green)	Actual field level margin lobes become visible in 1m aerial or Google Earth data.

Histograms based on lobe widths (at all scales) were created [Figure 26] and show that low silica lava exhibits a peak lobation mode at the smallest (under 50m) scale with secondary and tertiary levels of lobation occurring between 2-400m and around 1km respectively.

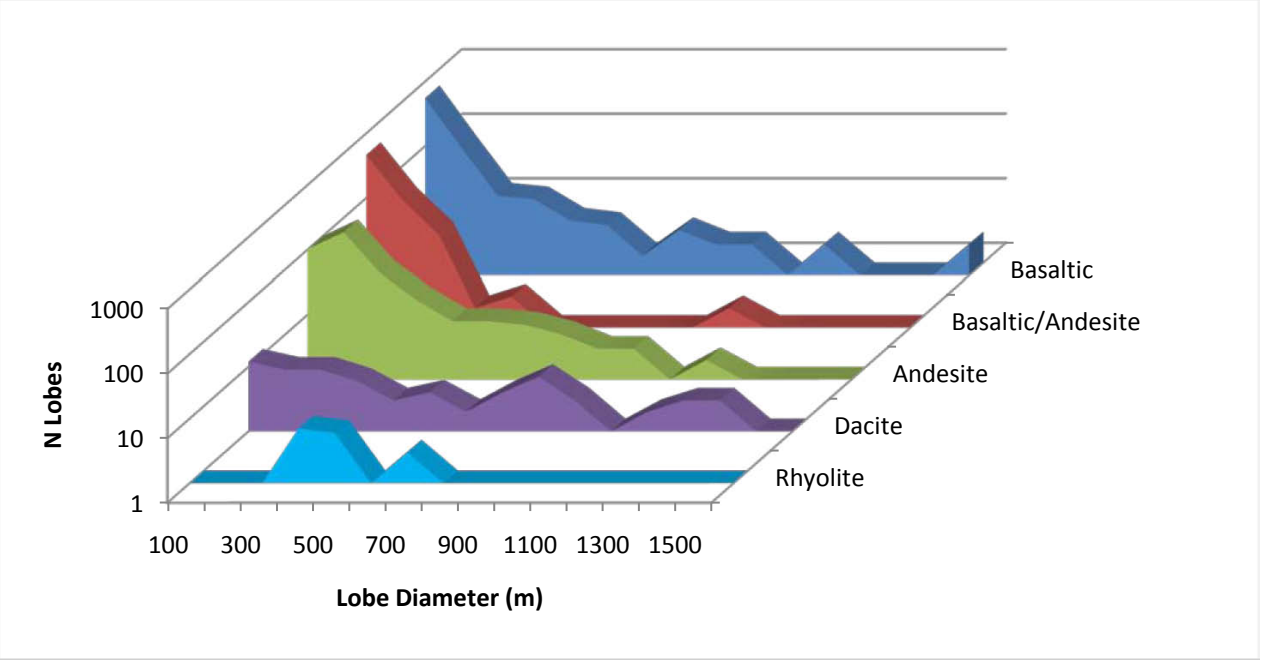

Figure 26: Lobe Diameters by Composition Histogram

Conversely, rhyolite lavas have only a single mode of lobation that occurs between 500m and 1km. At 30m or lower spatial resolutions, it was often difficult to distinguish between an intermediate lobe and a basaltic second level lobe. Summary values and margins of error are presented in Figure 27.

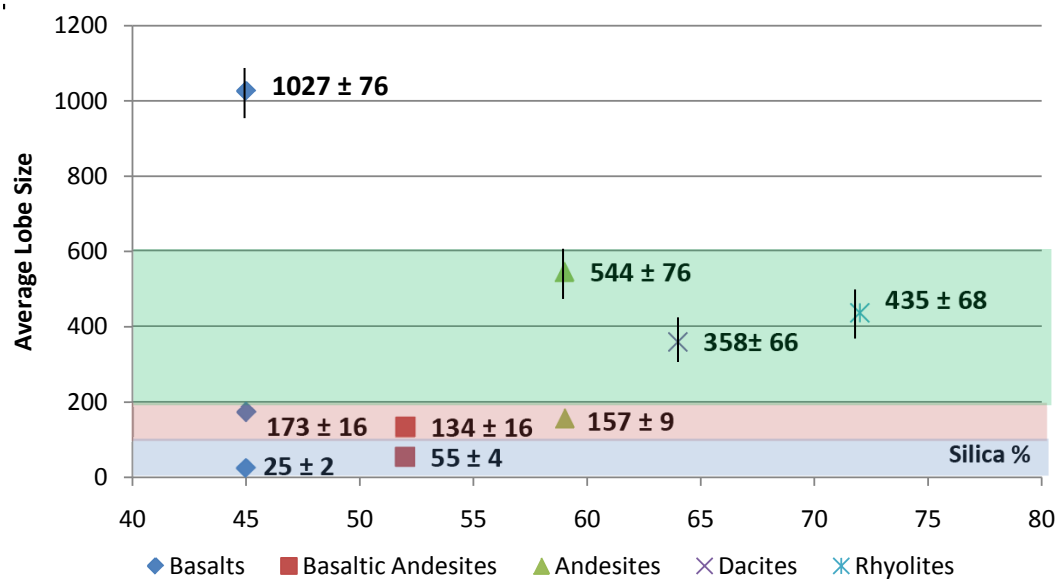

Figure 27: Mean lobe sizes by composition. Black lines represent 95% b.

A ratio of the lobe sizes at different 'levels of lobation' was calculated by dividing the average lobe size of the lower level into the average lobe size for the next higher level and are given in the chart below.

Table 3: Hierarcy of lobation ratio

	Lvl 1-Lvl 2	Lvl 2 – Lvl 3
Basaltic	6.92	5.93
Basaltic-Andesite	2.43	n/a
Andesite	3.46	n/a
Dacite	n/a	n/a
Rhyolite	n/a	n/a

Field and Error Analysis

The margins of error and physical basis for lobation morphology was analyzed during three field expeditions to several of this studies control dataset including flows at Belknap (2), Big Obsidian, Lava Butte, North Sister (3), Black Rock (2), Davis Lake, La Poruna, San Pedro (2), and Chao lava flows. GPS coordinates were taken at cleft points, the leading edge of the lobe, the lobe center (in the field, this was defined as the spot on top of the lobe where both clefts were at 180 degrees apart) and compared with satellite derived values. Cleft to cleft distances were measured in the field either via a ground wheel or a laser range finder. Intercleft and flow front angles were taken manually with a protractor. All field measurements were taken without any knowledge of the remotely measured values.

Field and remotely measured arc lengths differed by an average of 5m. Considering the remote measurements were made on 1m resolution data, this error seems appropriate. In the field, there were two notable sources of error. First, there was error inherent in the data gathering. Vegetation and fall from the leading edge of the flow often made it impossible to navigate a perfect arc with a ground wheel. [Figure 28]

Figure 28: Looking down from the top of a lobe at North Sister, OR – note the dense vegetation and wide debris field across the lobe front. Ground wheel measurements were difficult at best.

Secondly, arc measurements of large lobes necessitated using a laser range finder to take several straight line distances which were subsequently summed to get the full arc length. This digitization of an arc creates a small error across a large lobe. However, this variation is extremely small (+/- 5m) compared to the overall size of the flow lobe arcs [see Figure 8].

Field height measurements were taken one of two ways. GPS coordinates at the flow front and lobe top were taken. However, the vertical error of the GPS unit was often larger than the height of basaltic lobes. Lobe height values were also measured in the field using a laser range finder held at the lowest point and aimed at the highest visible point (or vice-versa where possible). By either method, field measurements of lobe height were consistently larger than those extracted from the digital elevation models. The Oregon dataset, which used 10m resolution vertical data, showed exactly a +/- 10m difference from field measurements. This could easily be due to slight errors in co-registration of the datasets. The Chilean data points, which were compared with a 30m interpolated ASTER DEM, differed from field measurements by an average of 16m.

Intercleft angle values that were clear in the satellite imagery were far less obvious on the ground. [Figure 29] Lines were drawn in the sand in front of the flow lobes paralleling the average direction of both flow lobes out from the cleft and that angle was measured manually with a protractor. However, windblown sand and debris fields at the base of each lobe often made the angle of emanation highly subjective. Consequently, angle measurements were highly varied in the field and rarely matched satellite predictions with errors of up to 20 degrees!

Figure 29: Intersection of three flow lobes at San Pedro, Chile – Note intercleft angles in the field above compared with in the remotely measured ASTER image below.

Erosional Climate Impact

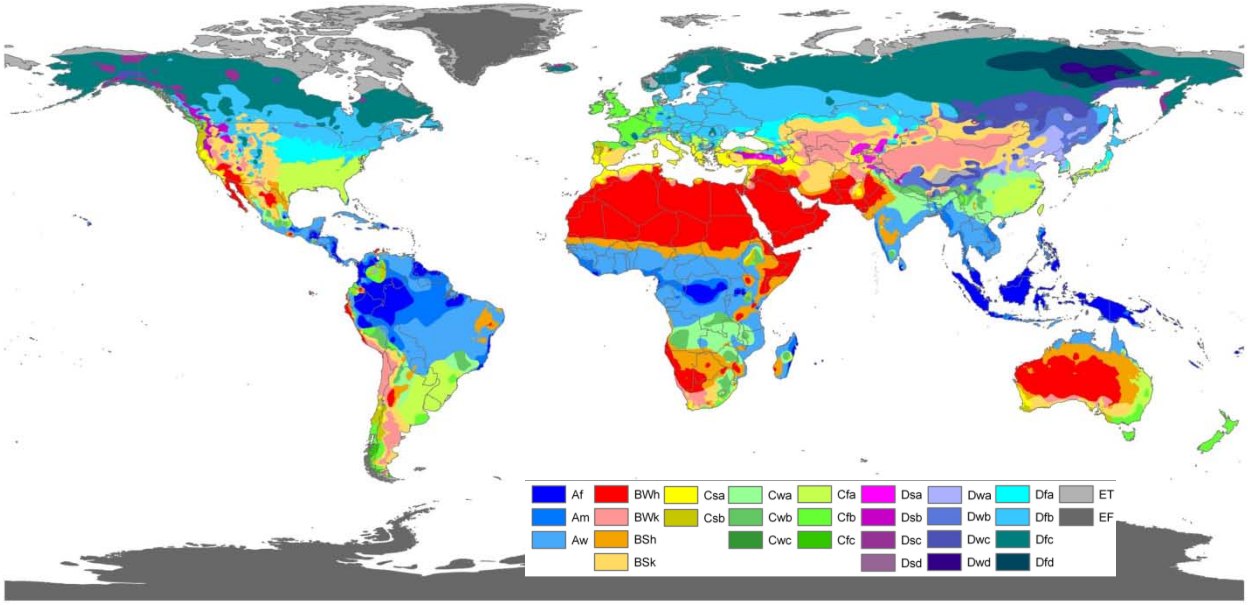

Figure 30: The Köppen climate classification map (Peel, 2007)

Köppen climate classifications based on Peel (2007) were used to tag each lava flow. [Figure 30 / Appendix 1] Flows in the Oregon Cascades were compared to flows of analogous composition in the hyper-arid Atacama desert of Chile to explore the erosional impact of climate on the final morphology of flow margin lobes.

The two field sites could not be more different. Oregon flows have significantly more fall rubble encircling and obscuring the margin and vegetation that has taken hold despite difficult growing conditions. [Figure 31] It is difficult to visually clearly distinguish between the natural flow margin and erosional fall.

Figure 31: The margin at Black Rock lava flow, Oregon Note the large trees/etc that obscure the margin

Conversely, the Chilean lava flow margins were generally pristine. Because of constant winds on the high Chilean desert, these flows often had loose material that had been blown into the clefts and over the margin. Nonetheless, the margins were often pristine, with considerably less fall and only the rarest hint of vegetation. [Figure 32]

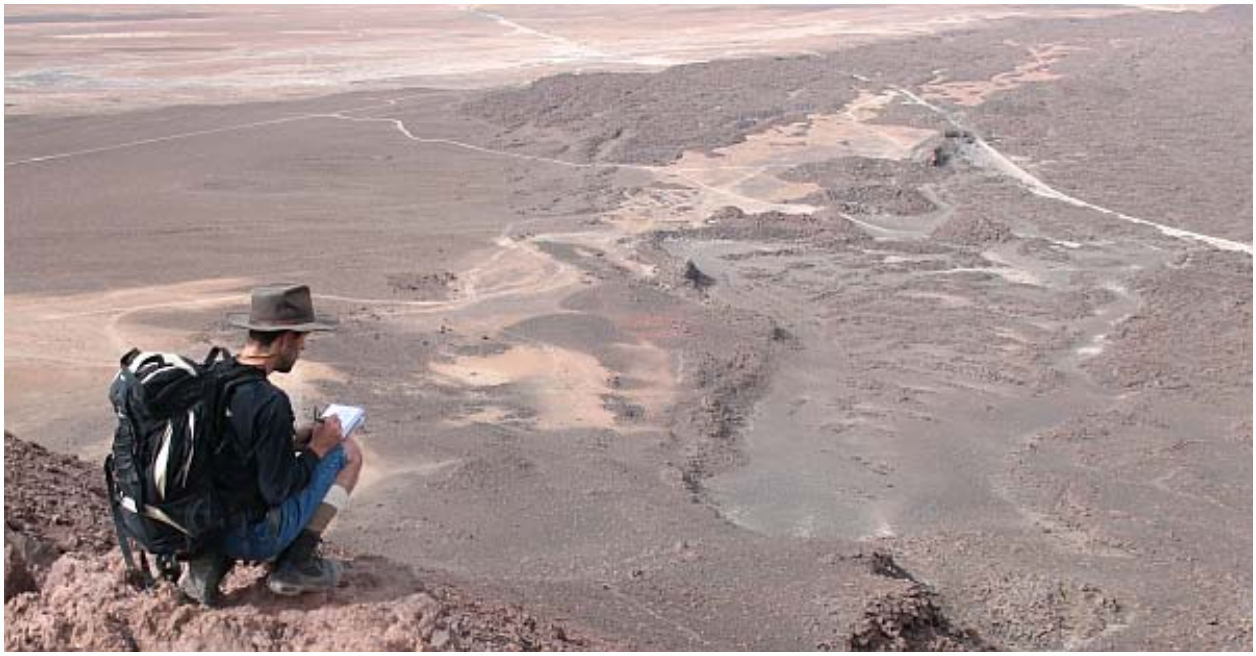

Figure 32: Margin lobe at La Poruna, Chile

Neither the constant directed aeolian erosion of the high Atacama desert winds nor the relentless fluvial onslaught of the Cascades modified flow margin lobes to the point beyond

where this type of modeling would be fruitful (at least not on the time scales of the flows observed). However, Oregon vegetation can hide things that would be clearly visible in the Atacama as seen in Case Study 3 below.

Interpretation and Analysis

Ultimately, the morphological variations that are found across lava flow margins are related to the lavas' viscosity. There are several factors that can increase the viscosity of lava including higher silica contents, decreased temperatures, and an increase in the amount of crystals in the lava. Correlations between lava morphology and calculated viscosity enable a deeper investigation into their relationship.

Using the Hagen-Poiseuille Law, there is a relationship between the growth rate of a lava dome, the size of the conduit, and the eruption rate that can be expressed as:

$$Q = \pi/8 * r4/\eta(\Delta p/l - \rho g) \quad (3)$$

where Q is the growth rate of the lava dome, r denotes the radius of the vent, Δp is the driving pressure, l is the vertical length of the vent, ρ is the density of the lava, η is the viscosity of the lava, and g is gravity acceleration. Yokoyama 2008 used the roughly linear relationship of Log Q to the SiO_2 content of lava to determine lava dome viscosity via:

$$log\ \eta \approx 0.087\ (SiO2) \quad (4)$$

Here we extrapolate this relationship to the full compositional spectrum of lava and explore four key morphological parameters that are directly related to lava viscosity lobe width and height (Wadge and Lopes, 1991), nearest neighbor distance (Welhan, 2002), and cleft formation over a given distance (Simpson, 1997).

Lobe width and nearest neighbor distance, both previously related to composition, not surprisingly, correlate well with calculated viscosity values. [Figure 33]

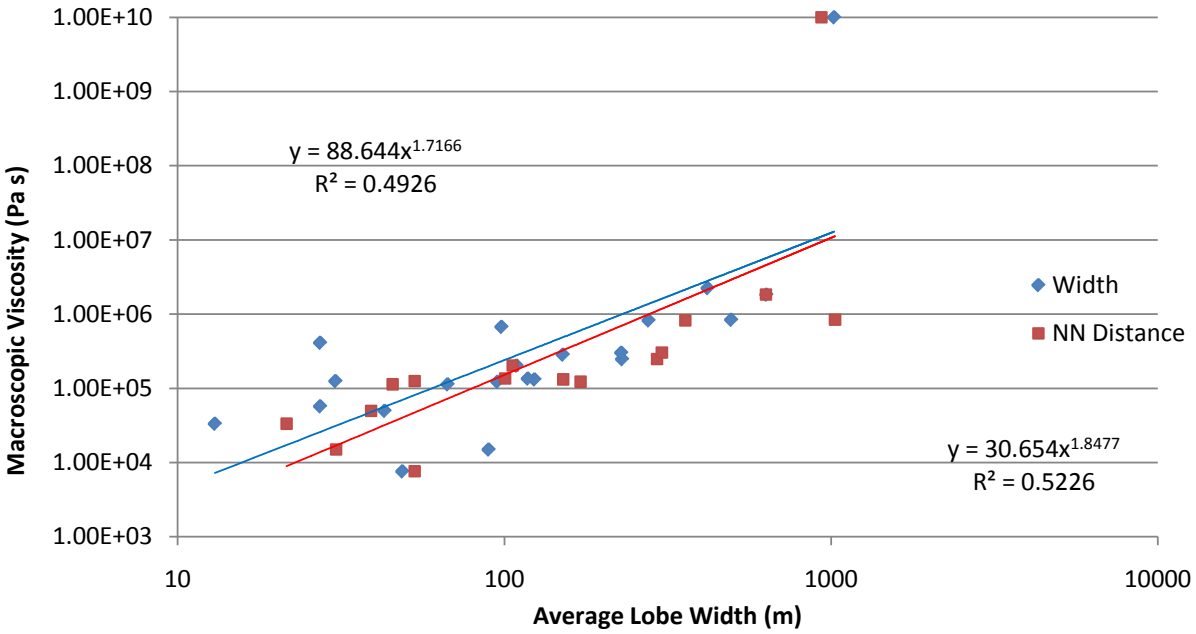

Figure 33: Viscosity vs Average Lobe Width

Average lobe heights also correspond well with calculated viscosity values. [Figure 34]

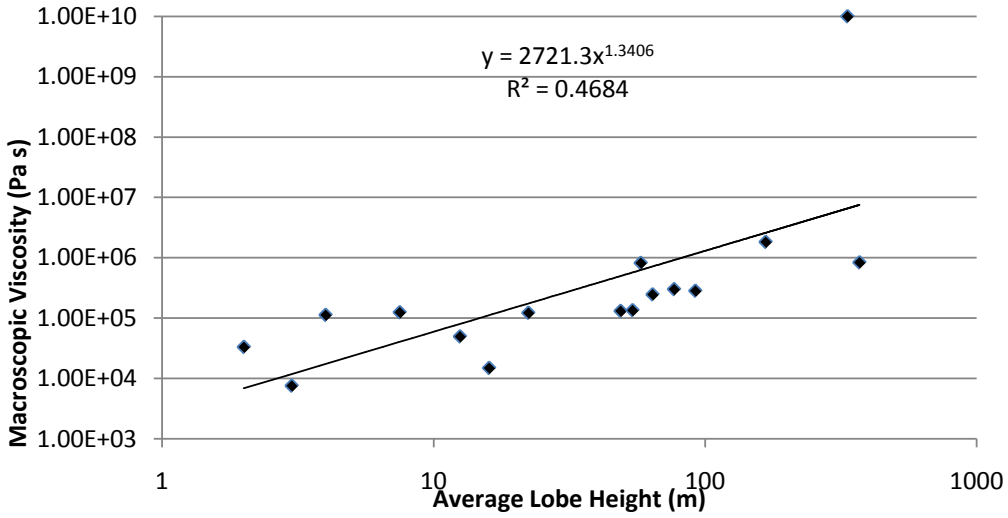

Figure 34: Viscosity vs. Average Lobe Height

At progressively higher viscosities, smaller scale feature formation is suppressed [Bruno, 1994] and cleft formation can fall as low as 1/km [Figure 35].

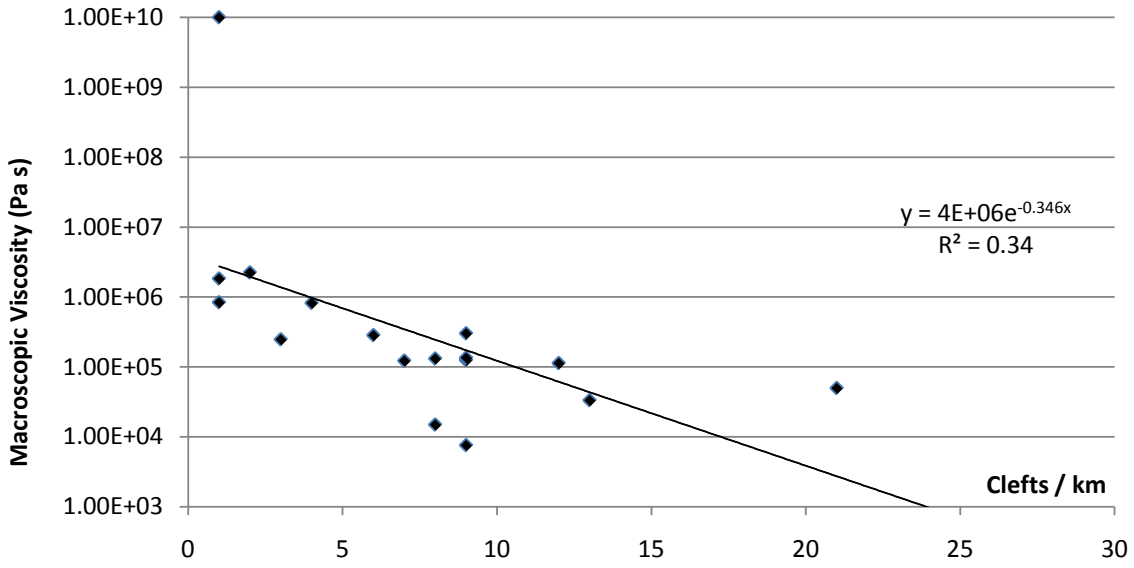

Figure 35: Clefts / km vs. Viscosity

Figure 36: Sample photo of the crystal rich Chao Dacite

Lower viscosities, however, progressively allow the ground to interact more with the lava and cleft formation correspondingly increases on several scales as seen in the hierarchy section above. This correlates well with previous fractal dimension work on flow margins. [Bruno, 94] Significant outliers in each chart correspond to the crystal rich Chao dacite. [Figure 36]

While only the foundational dataset of the LAMDA project, this dataset can already serve as a foundation for a plethora of possible higher order studies. For the purposes of this paper, I will focus on three case studies: A comparative analysis of two Bingham fluid equations (Hulme 74, Blake 90), an investigation of two prior aspect ratio proposals (Walker 71, Wadge & Lopes, 91), and an extrapolation analysis attempting to determine the composition of five lava flows based on their margin lobation.

Case Study 1: Bingham Fluid Equation Analysis

As an example of the utility of this dataset, yield strengths have been calculated two different ways \based on the satellite derived radii and height measurements and compared with known values. For this model, I used standard densities of 2.6 g/cm^3 for basalts, 2.41 g/cm^3 for andesites, 2.25 g/cm^3 for dacites, and 2.17 g/cm^3 for rhyolites and a standard Earth g of 9.8 m/s2. (Hall, 1996) Figure 37 plots equation (1) [Hulme, 1974] and equation (2) [Blake 1990] derived yield strength values with silica percentage.

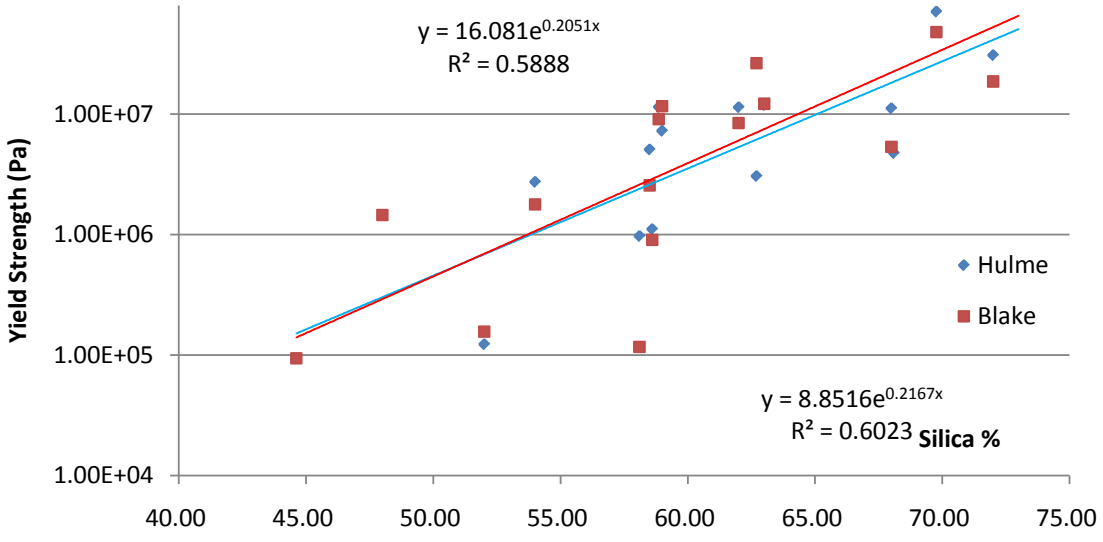

Figure 37: Yield Strength Predictions Using Hulme, 1974 and Blake, 1990

As a first order pass, the LAMDA morphometrics gave reasonable and relatively consistent results for yield strengths using both equations. Basaltic lobes were often beneath reliable height measurements and any error introduced in the height term would be compounded using the Blake method. Averaged lobe level local slope measurements were used where available in the Hulme equation rather than landscape level slopes. This may have introduced additional error in this model since local slope was shown in Figure 15 to be only a minor factor in final lobe morphology.

Case Study 2: Aspect Ratio versus Composition

Walker, 1973 presented a set of aspect ratios typical for given silica content. However, Walker's dataset was on the flow field scale not based on singular morphological features. Looking at purely distal lobes, Wadge and Lopes, 1991 found that irrespective of compositions, terrestrial lavas produced a very limited range of aspect ratios, which were uncorrelated with slope. The authors noted, however, that this may be due to relatively poor data resolution with the margins of error for height measurements exceeding the height of many low profile lava flows. This study attempted to examine this question again, using modern resolution data to calculate the aspect ratio of margin lobes, and confirms the Wadge and Lopes 1991 assessment.

Lobe aspect ratios for this study averaged .36 across compositions. [Figure 36] Remote height measurements of basaltic flows, however, still gave interpolated values below the resolution of the data and were not included with the exception of those lobes where height was determined in the field.

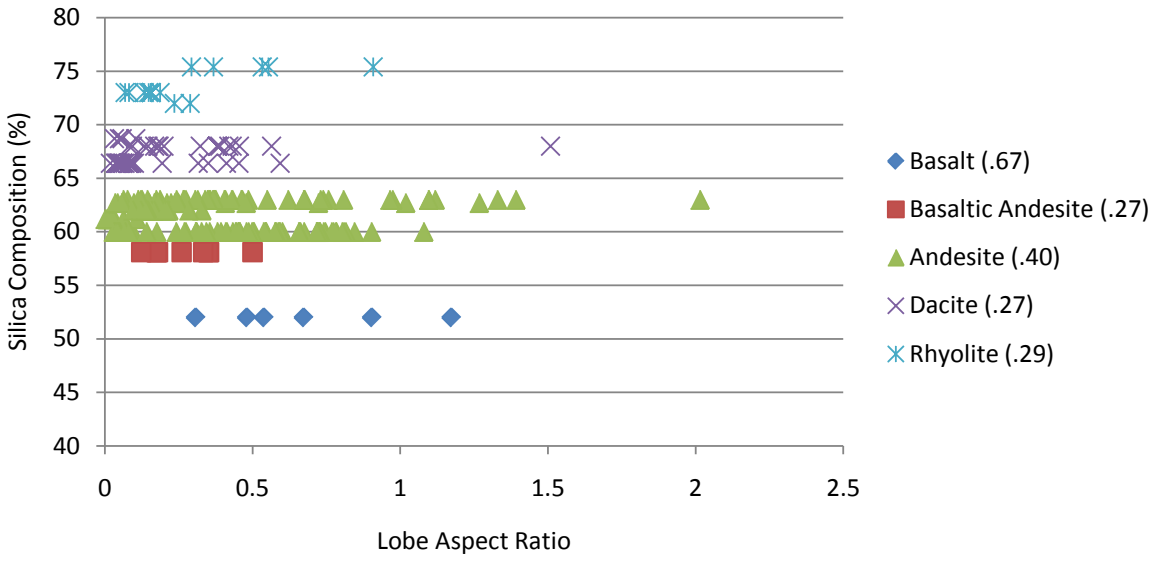

Figure 38: Aspect Ratio vs. Composition (Average Values in parenthesis)

Case Study 3: Terrestrial and LIDAR Interpolation

Terrestrial

Ultimately, the overarching goal of this comparative analysis was to create a modern data driven foundation for subsequent remote lava flow analysis. To test the 'predictability' of the model, three terrestrial lava flows were measured "blind" using the above methodology and compositional values were predicted and subsequently compared with literature based values. Four terrestrial flows (Glass Mountain, CA; SP Flow, AZ; and Hekla, Iceland) were randomly chosen for this study. Calculated SiO_2 values were derived using lobe v. compositional regression slope (see Figure 39 and equation 5) and the results are given in Table 3 below.

$$\boldsymbol{Lobe\ Width} = \mathbf{0.0117e0.1465}\boldsymbol{x} \Rightarrow \sim \mathbf{SiO_2\ Percentage} \qquad \mathbf{(5)}$$

Three of the four test flows were correctly classified categorically with relatively few lobes tested. The fourth flow, the dacite flow at Glass Mountain, was heavily contaminated with basalt [Eichelberger, 1978], which may account for the anomalously low lobe size for such an evolved composition. Adaption of this equation for extra-terrestrial investigations would simply require a recalibration using the appropriate gravity term.

Table 4: Terrestrial 'Blind' dataset

 Glass Mountain, CA (2 flows)	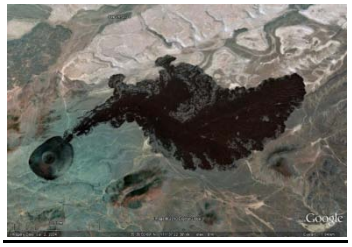 SP Flow, AZ	 Hekla, Iceland
Avg lobe size (Large) 419m (n=6) Average lobe size (small) 98m (n=17)	Average lobe size 95m (n=85)	Average lobe size 27m (n=13)
Calculated SiO_2 content **Large = 73%** **Small = 62%** **Actual SiO_2 content** **Large = 73%** **Small = 67%** *(Eichelberger, 1973)*	**Calculated SiO_2 content = 63%** **Actual SiO_2 content = 57%** *(Ulrich and Bailey, 1987)*	**Calculated SiO_2 content = 54%** **Actual SiO_2 content = 54.7%** *(Thorarinsson and Sigvaldason, 1972)*

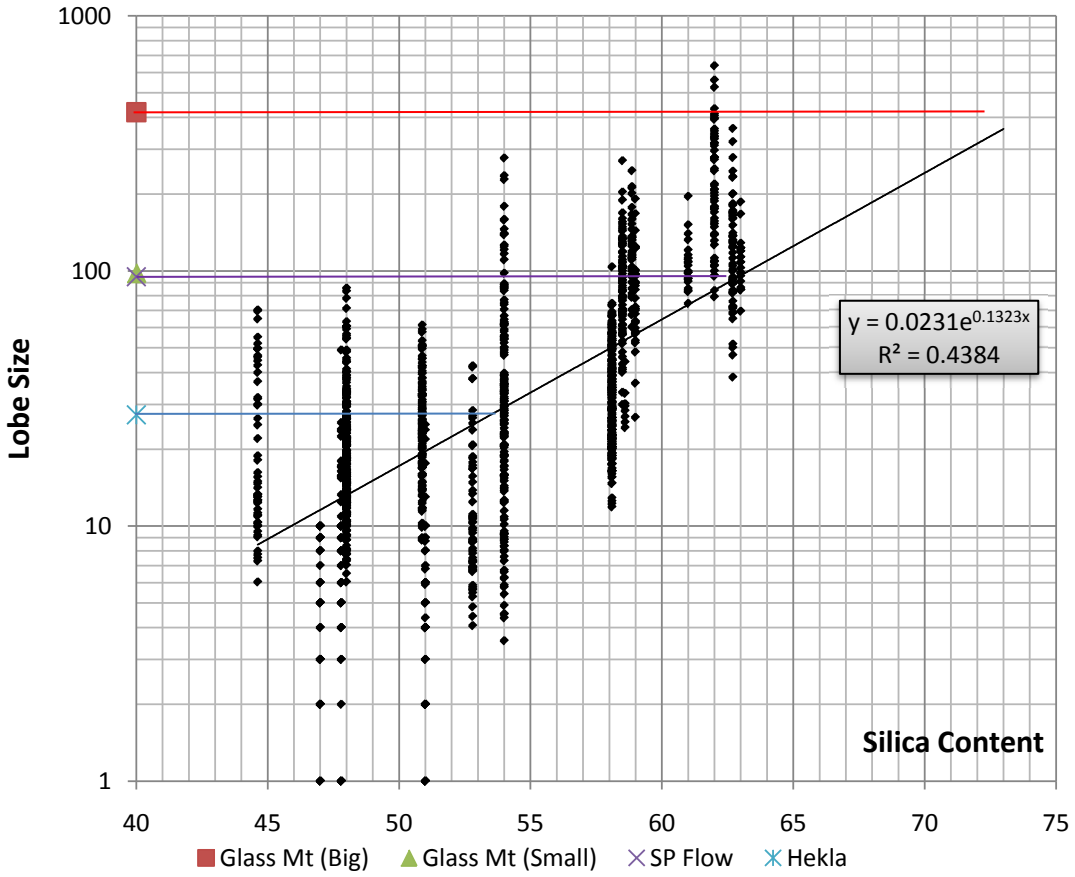

Figure 39: Lobe sizes for test flows and hypothesized compositional values

There is at least a ± 3% (silica %) margin of error due to resolution, rectification, and last minute data errors. Because there are additional factors, as discussed previously, that can alter the ultimate final size of a margin lobe, exact predictions are not to be expected, but by using the maximum, minimum, and average lobe sizes, a range of possible SiO2 contents can be determined.

LIDAR

Following on from this investigation, a lobation analysis was performed on a LIDAR (Light Detection And Ranging) derived bare earth image of Benchmark Butte, Oregon. By removing to vegetation, LIDAR exposes a geologic substructure that can then be examined using the same methodology. [Figure 40]

Figure 40: True Color and LIDAR images of Benchmark Butte, Oregon

Average lobe diameter for this flow is around 173 meters. Using equation (3), the SiO_2 content of this flow is estimated at 61%. The actual SiO2 compositional values for this flow is 65.8% seems reasonable based on morphological comparison with other flows near the same composition. These three case studies show the potential utility of this dataset for both the analysis of lava flow models and as a comparative morphological dataset.

Conclusions

The morphological features of a lava flow have been used in many previous studies to make a direct comparison between flows and features. Modern high resolution data and increased computing power now enable the collection and cataloging of lava morphological data on a planetary scale providing statistical significance and serving as the inductive foundation for planetary imagery studies as well as laboratory fluid studies. This is the simple concept behind the Lava Morphology Database (LAMDA).

The first morphological dataset for LAMDA, margin lobation, is a visibly distinct and useful feature for the remote study and analyses of lava flows. The height, width, and arc length of margin lobes directly, as well as the number of clefts/km, correlate with both the composition and viscosity of the lava but are relatively immune to even relatively large local topographic variation as well as vent distance.

Extrapolotaion of this data to unknown flows can accurately predict the type of lava in most circumstances, but vertical data resolution, margin erosion, and flow that come from the eruption of mixed magma are still potential sources of error. Expanding LAMDA to include additional features such as flow field size, ojives, block size distribution, etc., as well as adding further terrestrial baseline flows will increase the veracity and modeling potential of this project.

Literature Cited

- Baloga, S. M., Mouginis-Mark, P.J., and Glaze, L. S. (2003). The rheology of a long lava flow at Pavonis Mons, Mars. Journal of Geophysical Research 108(E7), 10.1029/2002JE001981.
- Blake S (1990) Viscoplastic models of lava domes. In: Fink JH (ed) IAVCEI Proc. in Volcanology, Vol. 2, 88-126.
- Blake S & Bruno, BC (2000) Modeling and Emplacement of Compound Lava Flows. Earth and Planetary Science Letters, Vol. 184, 1: 181-197.
- Bruno BC, Taylor GJ, Rowland SK, & Baloga, SM (1994) Quantifying the effect of rheology on lava-flow margins using fractal geometry. Bulletin of Volcanology, Vol. 56, 3:193 – 206.
- Bruno BC. (1994) Lava flow dynamics: Clues from fractal analysis. Ph.D. Dissertation, University of Hawaii. G Taylor, Chairperson.
- Carr, M.H. and R. Greeley. (1980). Volcanic features of Hawaii. A basis for comparison with Mars. NASA Technical Report SP403.
- Cattermole P (1987) Sequence, theological properties, and effusion rates of volcanic flows at Alba Patera, Mars. Journal of Geophysical Research, Vol. 92, B4: E553-60.
- Crisp J & Baloga S (1990) A method for estimating eruption rates of planetary lava flows. Icarus, Vol. 85, 512-15.
- Curtis SA, Clark, PE, Rilee, ML, Cheung, CY, Wesenberg, R, Dorband, J, Lunsford, A (2006) TET Rovers: An Approach For Exploring Rugged Terrains With Addressable Reconfigurable Technology. In: 2006 Lunar and Planetary Science Conference Proceedings. Available at: http://www.lpi.usra.edu/meetings/lpsc2006/pdf/1129 Accessed 28 March 2009
- Eicherberger, J. (1973) Origin of andesite and dacite: Evidence of mixing at Glass Mountain in California and at other circum-Pacific volcanoes. Geological Society of America Bulletin 1975;86;1381-1391
- Fiedor SJ & JM Ottino (2005) Mixing and segregation of granular matter: multi-lobe formation in time-periodic flows. Journal of Fluid Mechanics, 533:223-236.
- Fink JH & Fletcher RC (1978) Ropy pahoehoe: surface folding of a viscous fluid. Journal of Volcanology and Geothermal Research, 4:151-70.
- Fink, JH (1980) Surface folding and viscosity of rhyolite flows. Geology, 8:250-4.
- Fink, JH & Griffiths RW (1998) Morphology, eruption rates, and Rheology of lava domes: Insights from laboratory models. Journal of Geophysical Research, Vol. 103, B1: 527-545.
- Gregg TKP, Fink JH, Griffiths RW (1998) The formation of multiple fold generations on lava flow surfaces: influence of strain rate, cooling rate, and lava composition. Journal of Volcanology and Geothermal Research, 80:281–292.
- Gregg TKP & Fink JH (2000) A laboratory investigation into the effects of slope on lava flow morphology. Journal of Volcanology and Geothermal Research, 96:145–159.
- Griffiths RW & Fink JH (1992) The morphology of lava flows in planetary environments: predictions from analog experiments. Journal of Geophysical Research, Vol. 97, 19739–19748.
- Griffiths RW (2000) The Dynamics of Lava Flows. Annual Review of Fluid Mechanics. 32:477–518.
- Hall, Anthony, 1996. Igneous Petrology, 2nd Edition. Longman Group Limited, England.
- Härtel, C, Carlsson, F, Thunblom, M (2000) Analysis and direct numerical simulation of the flow at a gravity-current head. Part 2. The lobe-and-cleft instability. Journal of Fluid Mechanics, 418:213-229.
- Head, James W., et.al. (1992) Venus Volcanism: Classification of Volcanic Features and Structures, Associations, and Global Distribution from Magellan Data. Journal Of Geophysical Research, Vol. 97, No. E8, pp. 13,153-13,197. doi:10.1029/92JE01273
- Head, James W., et.al. (2009) Volcanism on Mercury: Evidence from the first MESSENGER flyby for extrusive and explosive activity and the volcanic origin of plains, Earth and Planetary Science Letters, Volume 285, Issues 3-4, MESSENGER's First Flyby of Mercury, Pages 227-242, ISSN 0012-821X, DOI: 10.1016/j.epsl.2009.03.007.
- Hulme G. (1974) The interpretation of lava flow morphology. Geophysical Journal of the Royal Astronomical Society, 39:361–83.
- Hulme, G and G. Fielder (1977) Effusion Rates and Rheology of Lunar Lavas. Philosophical Transactions of the Royal Society of London. Series A, Mathematical and Physical Sciences, Vol. 285, No. 1327, The Moon: A New Appraisal from Space Missions and Laboratory Analyses (Mar. 31, 1977), pp. 227-234.

- Iverson, R (1997) The Physics of Debris Flows. Reviews of Geophysics. 25:245-296.
- Jegou I, Savoye B, Droz L, and Pirmez C (2006) Stages of Construction of the Distal Lobes of the Amazon Deep Sea Fan. American Association of Petroleum Geologists *2006 Conference Poster #90052* .
- Kilburn CRJ, Lopes RM (1991) General patterns of flow field growth: Aa and blocky lavas. Journal Of Geophysical Research. Vol. 96, B12: 19721–19732.
- Kilburn, C (2000) Lava Flows and Flow Fields. In: Sigurdsson H (ed) Encyclopedia of Volcanoes, Academic Press, San Diego, California, pp 291-305.
- Lopes, R (1993) Extraterrestrial Lavas. In: Kilburn C (ed) Active Lavas: Monitoring and Modeling, Taylor and Francis, pp 107-143.
- Lopes-Gautier R, et.al. (1991) Martian lavas: Three complementary remote sensing techniques to derive flow properties. In: NASA Technical Report #19940011893 Proceedings of the Twenty-Fourth Lunar and Planetary Science Conference. Part 2 G-M pp 899-900.
- Lopes, R.M.C. et.al. (2007) Cryovolcanic features on Titan's surface as revealed by the Cassini Titan Radar Mapper, Icarus, Volume 186, Issue 2, Pages 395-412, ISSN 0019-1035, DOI: 10.1016/j.icarus.2006.09.006.
- Lum, C. C. L., Leeman, W. P., Foland, K. A., Kargel, J. A., and Fitton, J. G., 1989, Isotopic variations in continental basaltic lavas as indicators of mantle heterogeneity: Examples from the western U.S. Cordillera: Journal of Geophysical Research, v. 94, no. B6, p. 7871-7884.
- McBirney AR & Murase T (1984) Rheological Properties of Magmas. Annual Review of Earth and Planetary Sciences, 12:337-357.
- McElwaine JN & Patterson MD (2004) Lobe And Cleft Formation At The Head Of A Gravity Current. In: Proceedings of the XXI International Congress of Theoretical and Applied Mechanics, Warsaw, Poland. FM9S_12396.
- Meyer JD & White SM (2007) Lava morphology mapping by expert system classification of high resolution side-scan sonar imagery from the East Pacific Rise, 9° –10° N. Marine Geophysical Research, 28:81-93.
- Miyamoto H & Crown D (2006) A simplified two-component model for the lateral growth of pahoehoe lobes. Journal of Volcanology and Geothermal Research, Vol. 157, 4:331-342.
- Moore HJ, Arthur DWG, Schaber GG (1978) Yield strengths of flows on the Earth, Mars, and Moon. In: Proceedings of the Ninth Lunar and Planetary Science Conference. pp. 3351-78.
- Murase T & McBirney AR (1973) Properties of some common igneous rocks and their melts at high temperatures. Geologic Society of America Bulletin 84:3563-3592.
- O'Callaghan, L.J., & Francis, P.W., 1986. Volcanological and petrological evolution of San Pedro volcano, Provincia El Loa, North Chile. J. Geol. Soc. Lond. 143, p275-286
- Peckyno, R and S de Silva. "LAMDA - The Lava Morphology Database" Proceedings of the GSA Annual Meeting. October 2009, Portland, OR.
- Peckyno, R, S de Silva, R Lopes, and D Pieri. "The Lava Flow Morphology Database (LAMDA)" Abstract and Poster, AGU Annual Meeting. December 2009, San Francisco, CA.
- Peel MC, Finlayson BL, & McMahon TA (2007) Updated world map of the Köppen-Geiger climate classification. Hydrology and Earth System Science, 11:1633–1644.
- Punkari M (1980) The ice lobes of the Scandinavian ice sheet during the deglaciation in Finland. Boreas, Vol. 9, 4:307 – 310.
- Rossi, MJ and A. Gudmundsson. (1996) The morphology and formation of flow-lobe tumuli on Icelandic shield volcanoes, Journal of Volcanology and Geothermal Research, Volume 72, Issues 3-4, Pages 291-308, ISSN 0377-0273, DOI: 10.1016/0377-0273(96)00014-5.
- Shaw HR, Wright TL, Peck DL, & Okamura R (1968) The viscosity of basaltic magmas: an analysis of field measurements in Makaopuhi lava lake, Hawaii. American Journal of Science, 266:225-264.
- Simpson JE (1972) Effects of the lower boundary on the head of a gravity current. Journal of Fluid Mechanics, 53:759-768.
- Simpson JE (1997) Gravity Currents in the Environment and the Laboratory, 2nd ed. Cambridge University Press, ISBN#0521561094.
- Theilig E & Greeley R (1986) Lava Flows on Mars: Analysis of Small Surface Features and Comparisons with Terrestrial Analogs. Journal of Geophysical Research, Vol. 91, B13:E193-E206.

- Thorarinsson, S., and Sigvaldason, G.R., (1972) The Hekla eruption of 1970: Bull. Volcanol., v. 36, p. 269-288
- Ulrich, G.E. and N. G. Bailey (1987) Geologic Map of SP Mountain part of San Francisco Volcanic Field, North-Central Arizona. USGS Misc.Field Map MF-1956.
- USGS Open-File Report 2005-1305 Preliminary integrated geologic map databases for the United States - western states: California, Nevada, Arizona, Washington, Oregon, Idaho, and Utah.
- Ventura G & Vilardo G (2008) Emplacement mechanism of gravity flows inferred from high resolution LIDAR data: The 1944 Somma–Vesuvius lava flow (Italy). Geomorphology, doi:10.1016/j.geomorph.2007.06.005.
- Wadge G & Lopes RMC (1991) The Lobes of Lava Flows on Earth and Olympus Mons, Mars. Bulletin of Volcanology, 54:10-24.
- Walker G (1973) Lengths of lava flows. Philosophical Transactions of the Royal Society of London, A274:107:118.
- Warner, N & Gregg TKP. (2003) Evolved lavas on Mars - Observations from southwest Arsia Mons and Sabancaya volcano, Peru. Journal of Geophysical Research, Vol. 108, E10:5112.
- Welhan JA, Johannesen CM, Reeves K, Clemo T, Glover JA & Bosworth K (2002) Morphology of inflated pahoehoe lavas and spatial architecture of their porous and permeable zones, eastern Snake River Plain, Idaho In: Geological Society of America Special Paper 353, p. 135-150.
- Williams, D. A., A. G. Davies, L. P. Keszthelyi, and R. Greeley (2001), The summer 1997 eruption at Pillan Patera on Io: Implications for ultrabasic lava flow emplacement, J. Geophys. Res., 106, 33,105–33,119, doi:10.1029/2000JE001339.
- Yokoyama, I. (2005) Growth rates of lava domes with respect to viscosity of magmas. Annals of Geophysics, Vol. 48, n. 6.
- Zimbelman JR (1985) Estimates of rheologic properties for flows on the Martian volcano Ascreus Mons. Journal of Geophysical Research, 90:D157-D162.
- Zimbelman JR, et.al. Emplacement of the 1907 Mauna Loa basalt flow as derived from precision topography and satellite imaging. (2008) Journal of Volcanology and Geothermal Research 177:837-847

Appendix A: Dataset Table

Volcano	Composition	Location	Climate Class*	Lvl1 Lobes
Akita-Komagatake	Andesite	Honshu, Japan	Dfa	8
Belknap	Basaltic	Oregon	Dsb	63
Big Obsidian Flow	Rhyolite	Oregon	BWk	3
Black Rock Flow (3)	Andesite	Oregon	Dsb	64
Ceboruco	Dacite	México	Csa	10
Cerro Chascon	Rhyolite	SW Bolivia	BWk	8
Chao	Dacite	Northern Chile	BWk	8
Davis Lake Flow	Andesite	Oregon	Dsb	40
Four Craters	Basaltic	Oregon	BSk	240
Glass Mountain (2)	Rhyolite and Dacite	California	Dsb	24
Helka	B, BA	Iceland	Dfc	13
La Poruna	Basaltic Andesite	Northern Chile	BWk	316
North Sister (4)	Basaltic Andesite	Oregon	Dsb	168
Payun Matru	Trachybasalt	Argentina	BWk	17
San Pedro (2)	Andesite	Northern Chile	BWk	62
Shasta (2)	Andesite	California	Dsb	18
Socompa (3)	Hb. Andesite	Northern Chile-Argentina	BSk	71
SP Flow	Andesite	Arizona	Dsb	85
Totals				1218

*Köppen Climate Classification from (Peel, 2007)

Appendix B: Dataset Maps

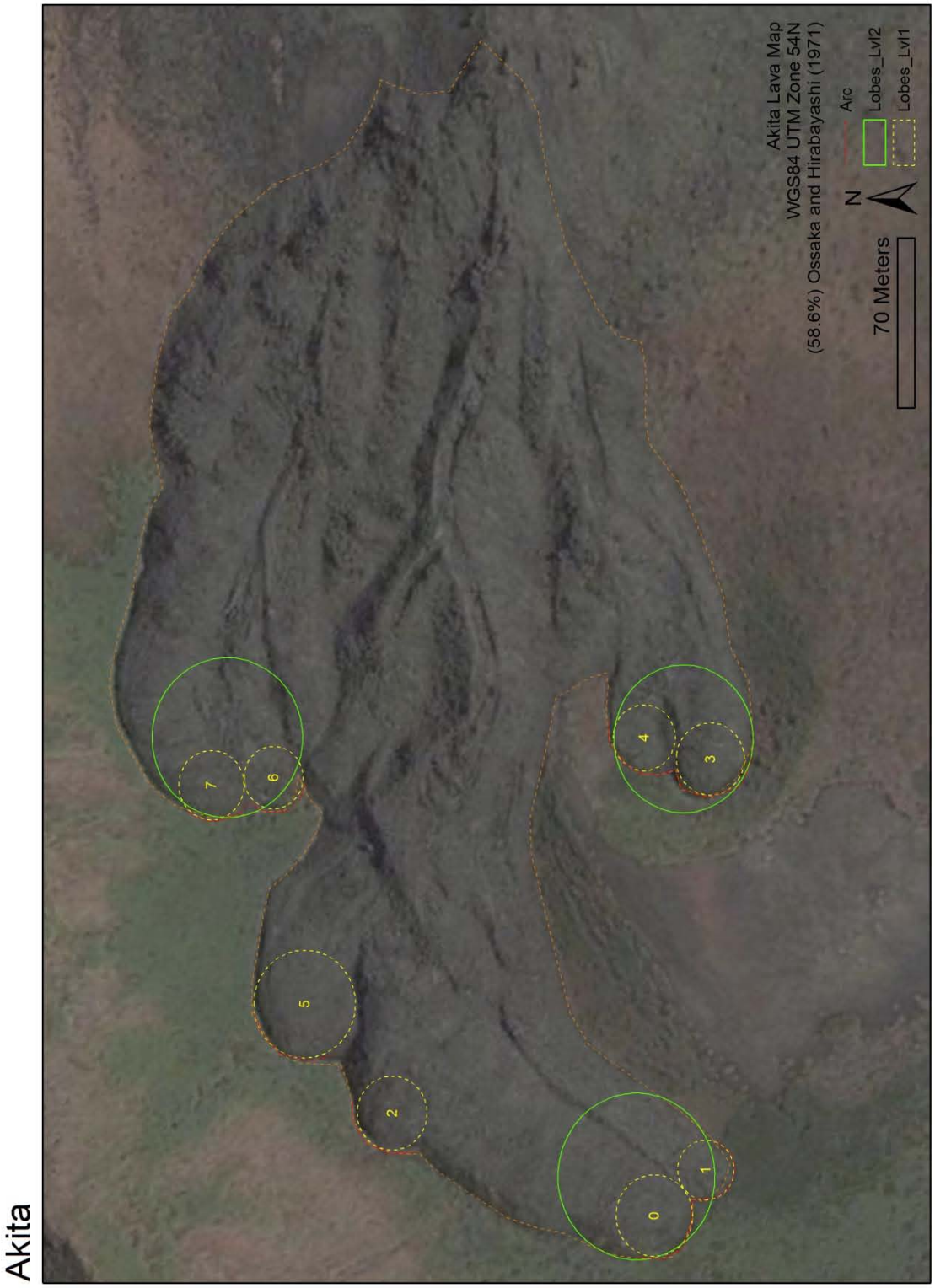

Belknap Distal Lobes

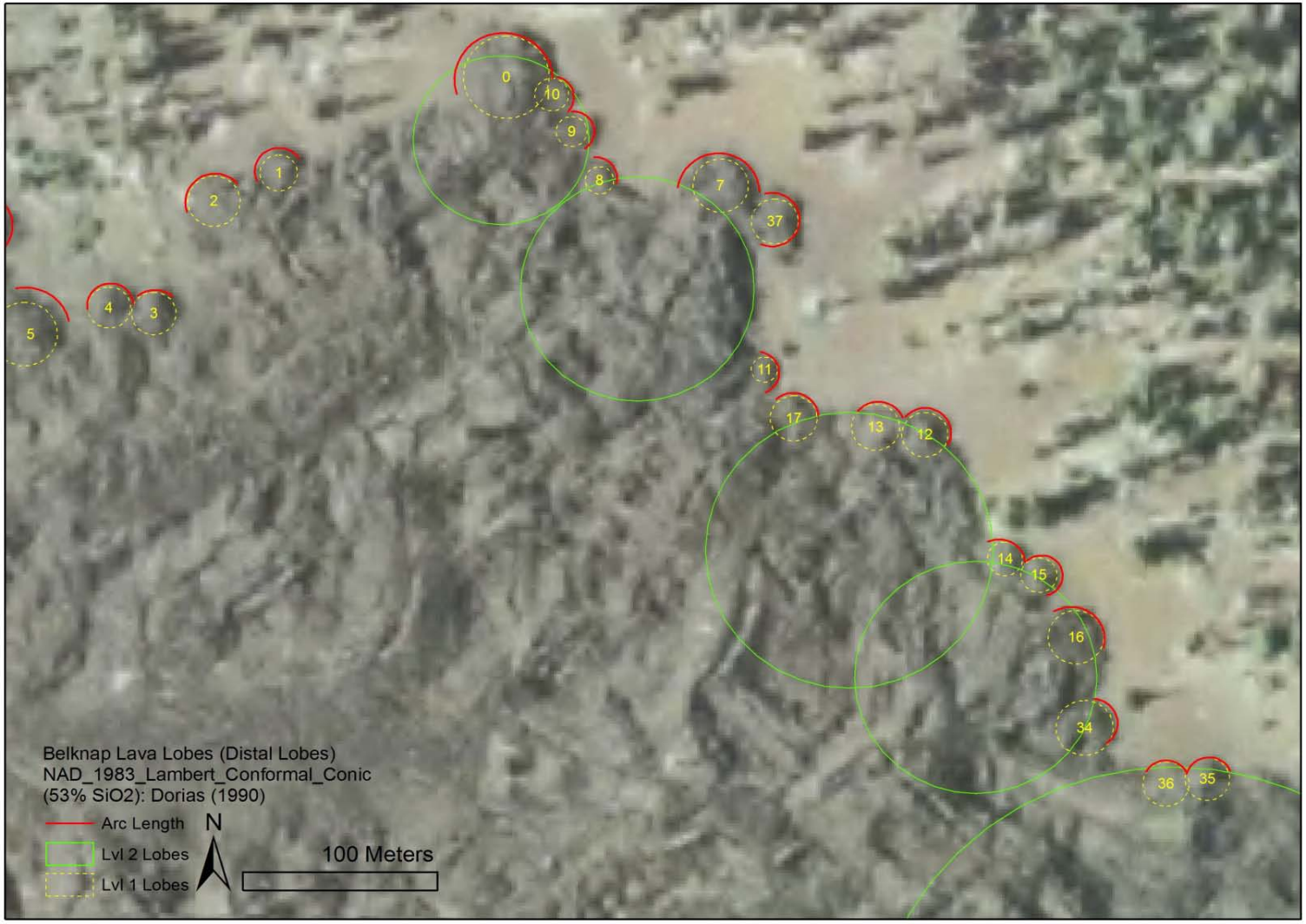

Big Obsidian Flow

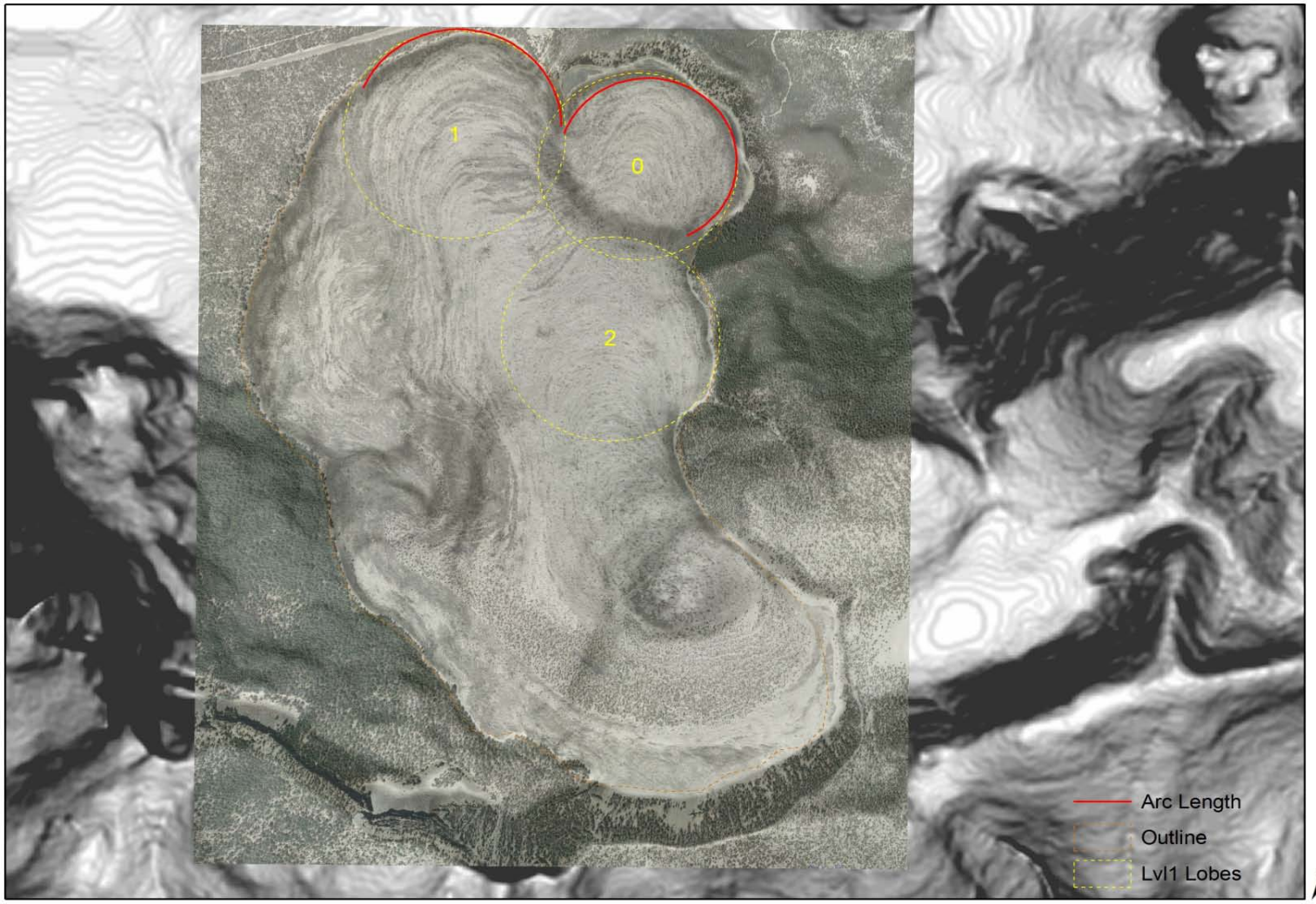

Big Obsidian Lava Lobes
NAD_1983_Lambert_Conformal_Conic
(72% SiO2): Laidley and Mackey (1971)

'Black Rock' South

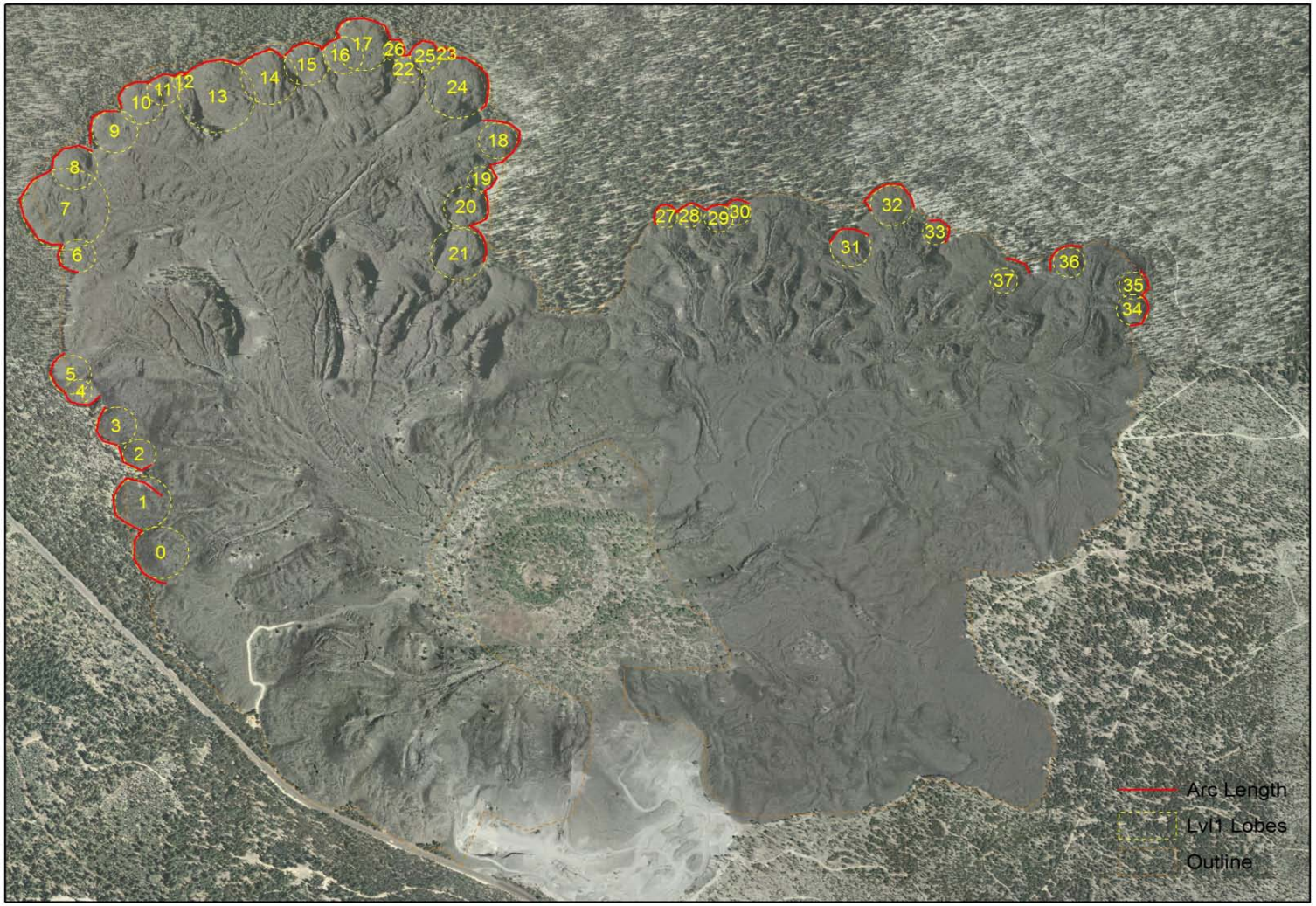

'Black Rock' South Lava Flow
NAD_1983_Lambert_Conformal_Conic
(58.99% SiO2) MacLeod and Sherrod, 1992

Ceboruco - 1870 Dacite

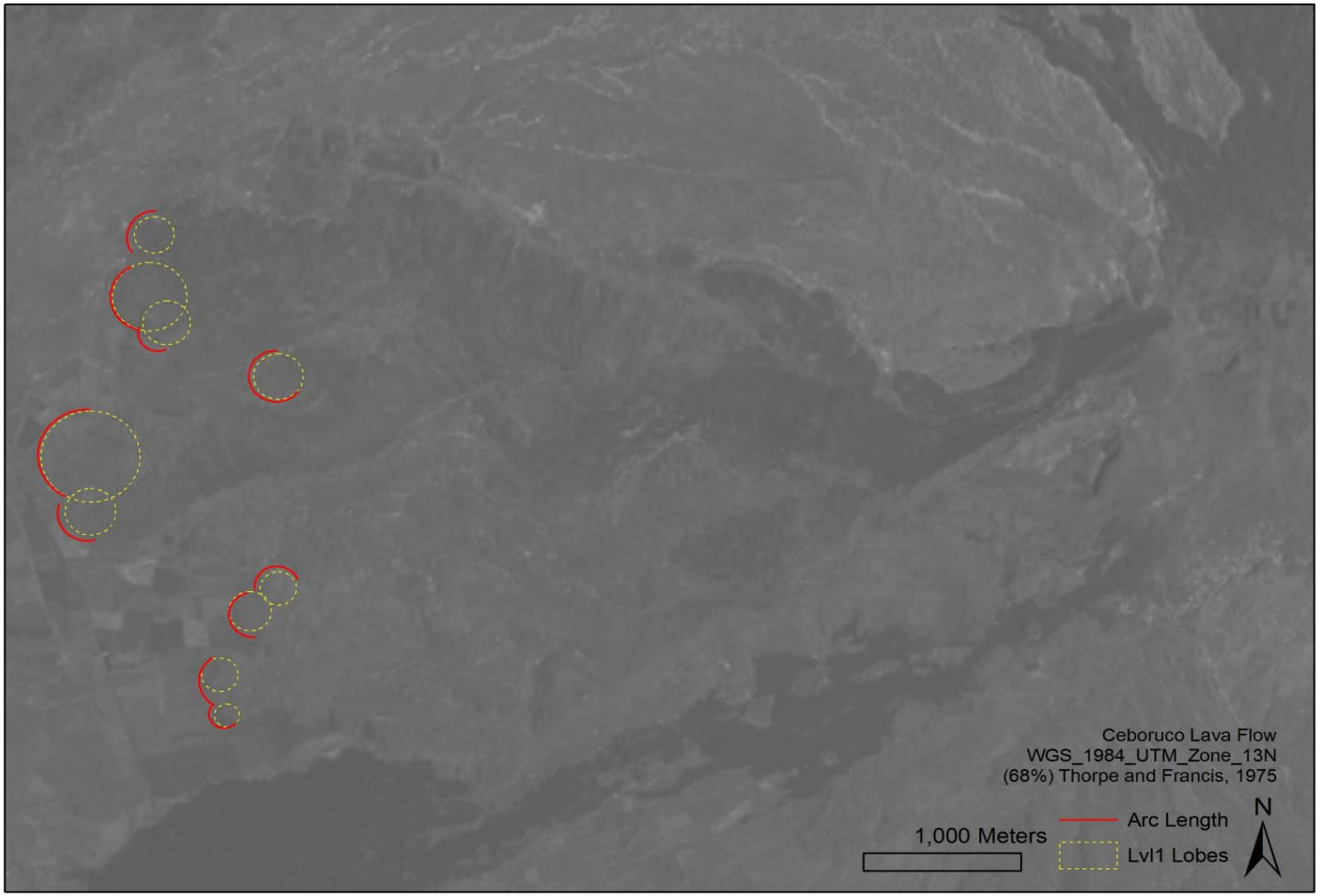

Chao

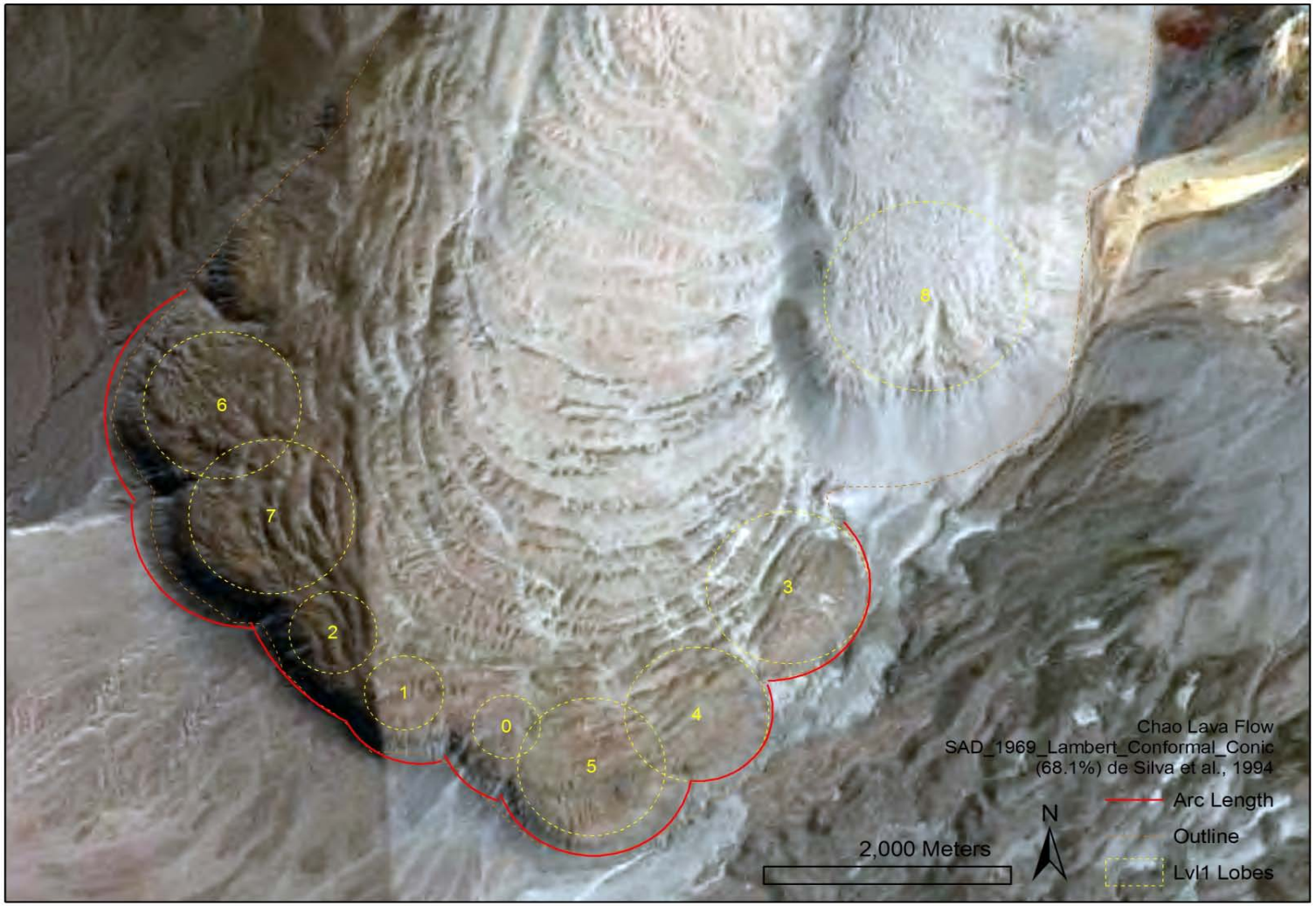
6
6
7
3
2
1
0
5
4
Chao Lava Flow
SAD_1969_Lambert_Conformal_Conic
(68.1%) de Silva et al., 1994
Arc Length
Outline
Lvl1 Lobes
N
2,000 Meters

Chascon


5
0
2
1
3
7
6
4
Chascon Lava Flow
SAD_1969_Lambert_Conformal_Conic
(68%) de Silva et al, 1994
1,000
Meters
N
Lvl1_lobes
Outline

Davis Lake

Davis Lake Lava
NAD_1983_Lambert_Conformal_Conic
(58.86%) MacLeod and Sherrod, 1992

Four Craters

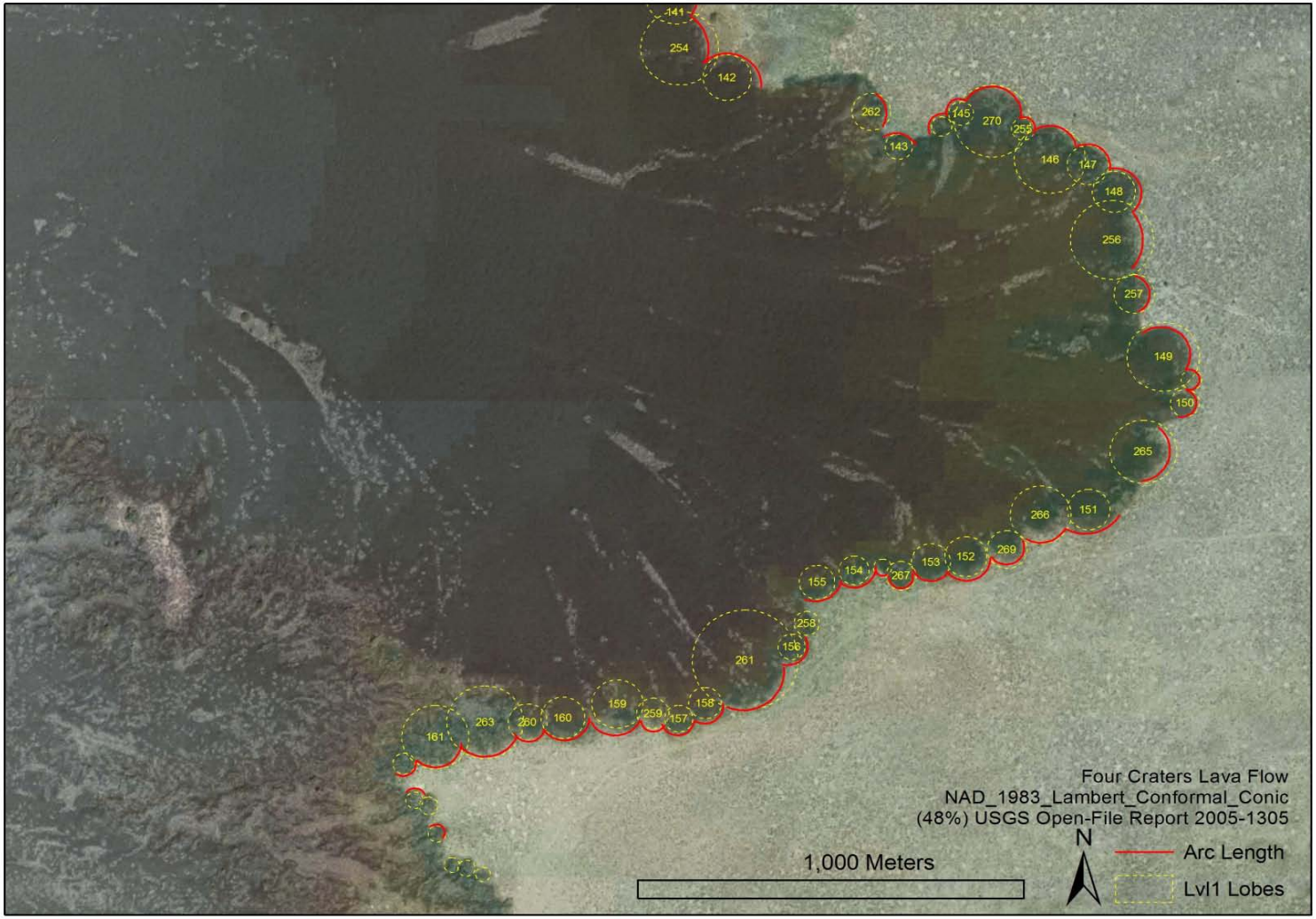

Glass Mountain

Glass Mountain Lava Flows
NAD_1983_California_Teale_Albers
SiO2 (73% / 67%) Eichelberger, 1973

N

1,000 Meters

La Poruna

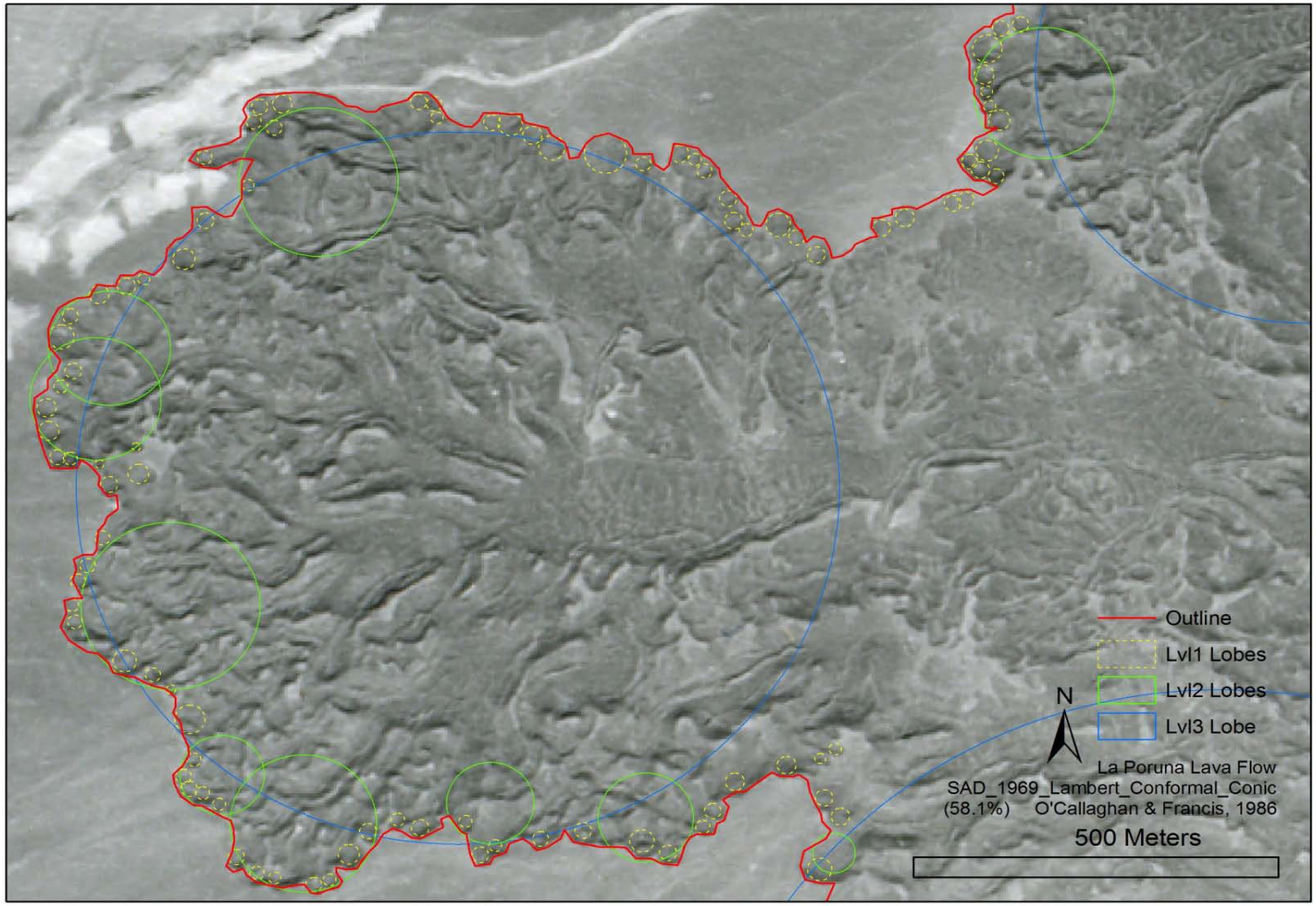
Outline
Lvl1 Lobes
Lvl2 Lobes
Lvl3 Lobe
N
La Poruna Lava Flow
SAD_1969_Lambert_Conformal_Conic
(58.1%) O'Callaghan & Francis, 1986
500 Meters

Lunar Crater, Nevada

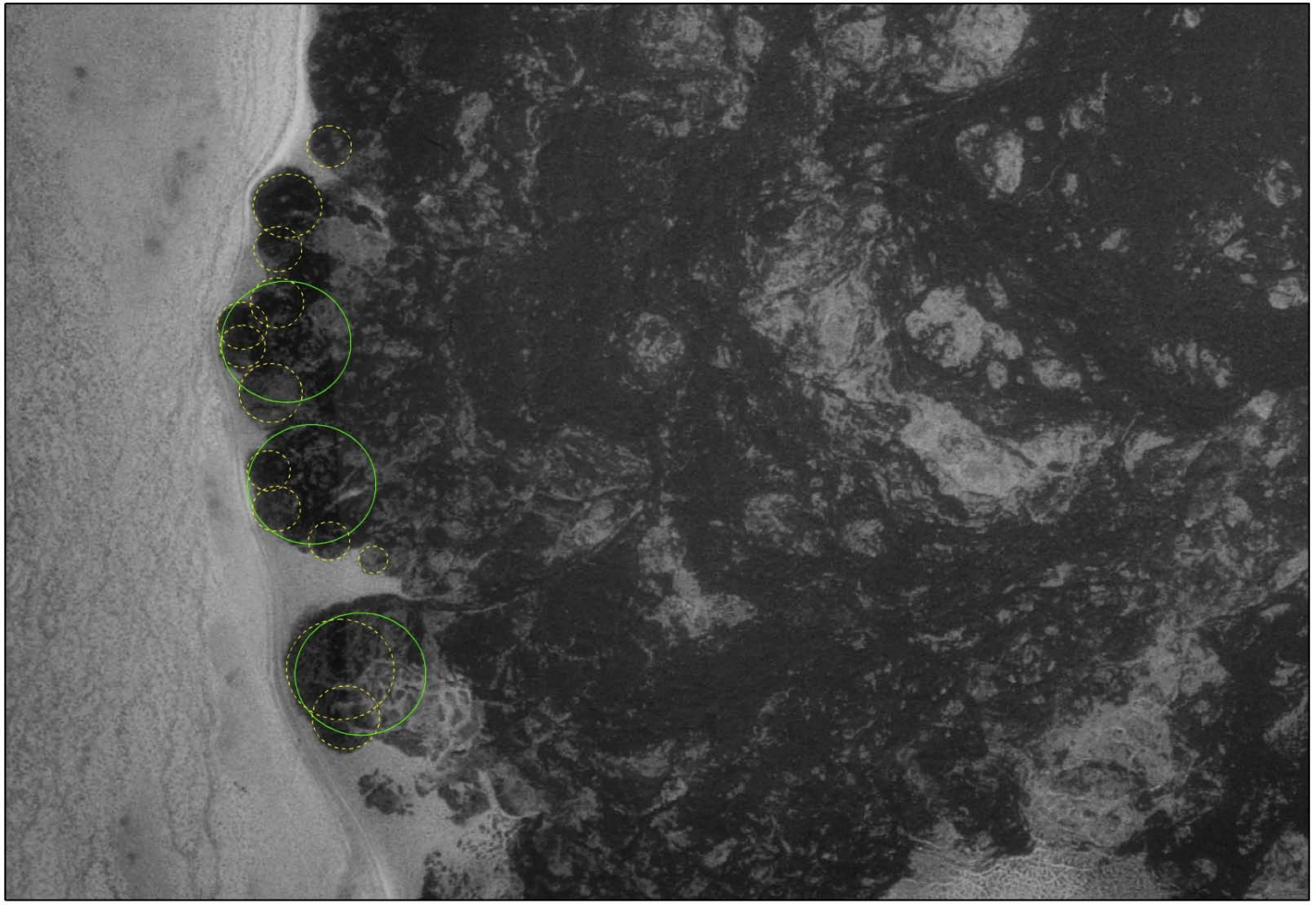

Lunar Crater Lava Lobes
NAD_1983_UTM_Zone_11N
44.62% (Lum et.al, 1989)

North Sister

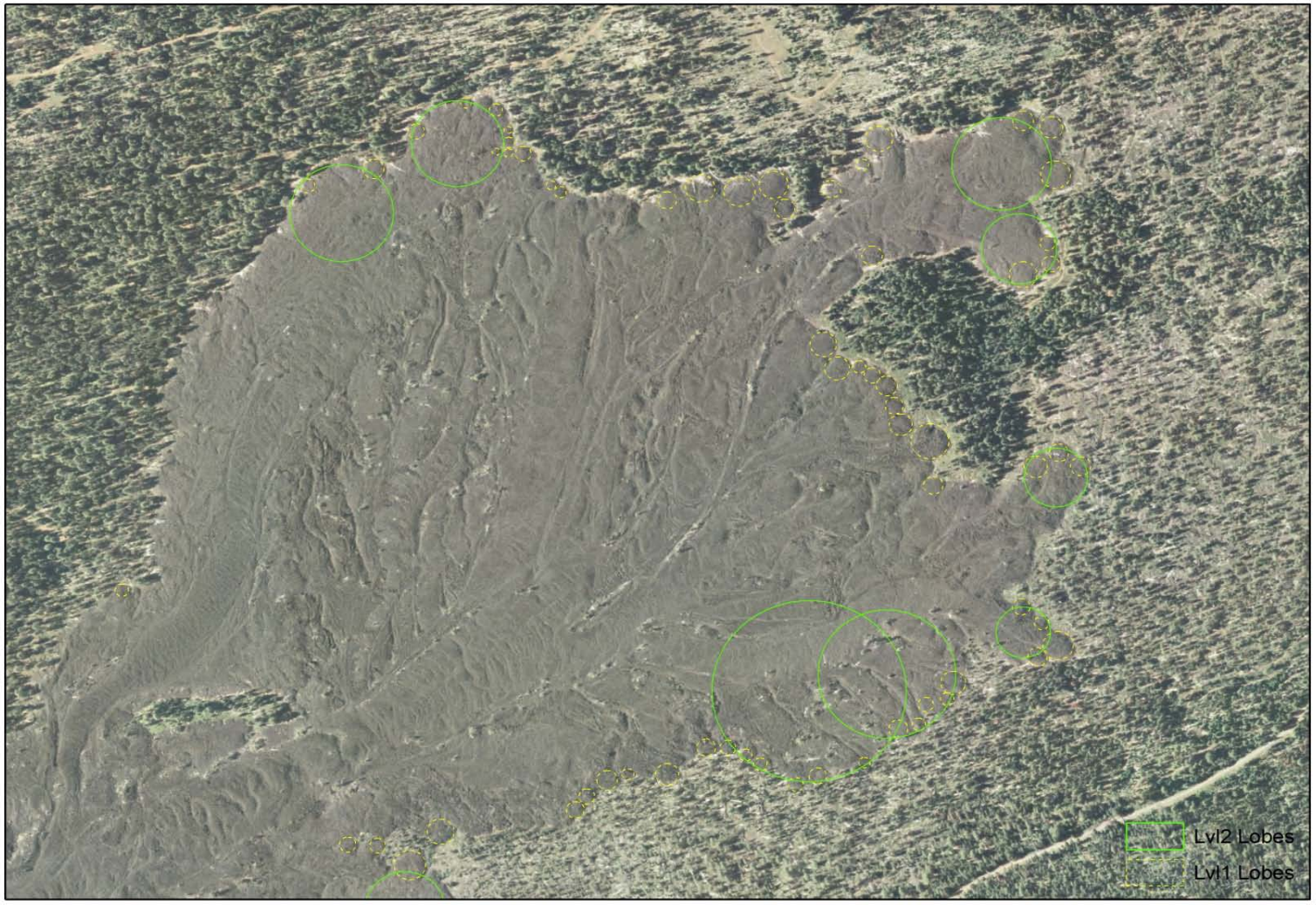

North Sister Lava Lobes
NAD_1983_Lambert_Conformal_Conic
(53%) Schmidt, 2005

Payun Matru

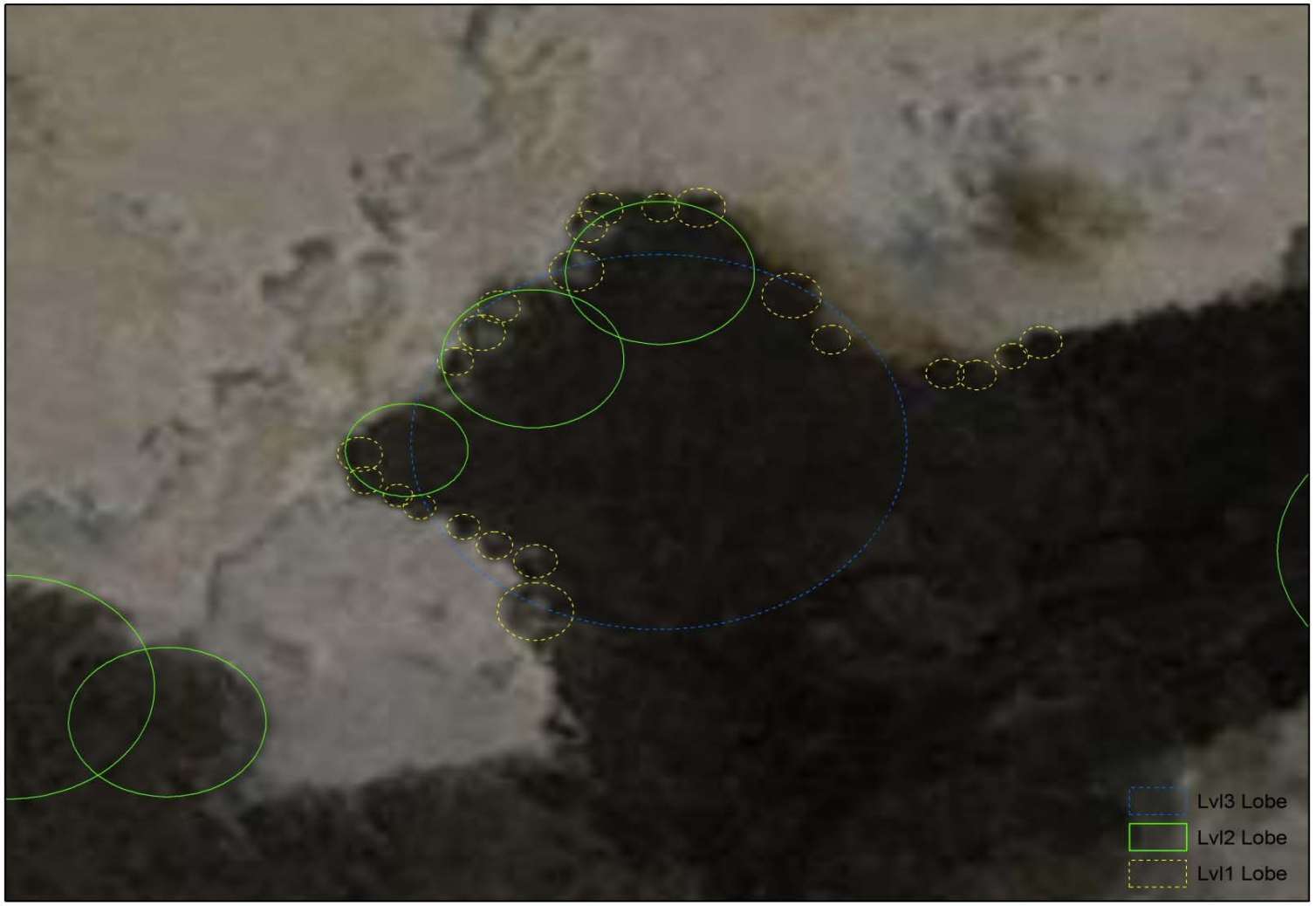

Payun Matru Lava Lobes
SAD_1969_Lambert_Conformal_Conic
(61%) Gonzales, 1972

San Pedro

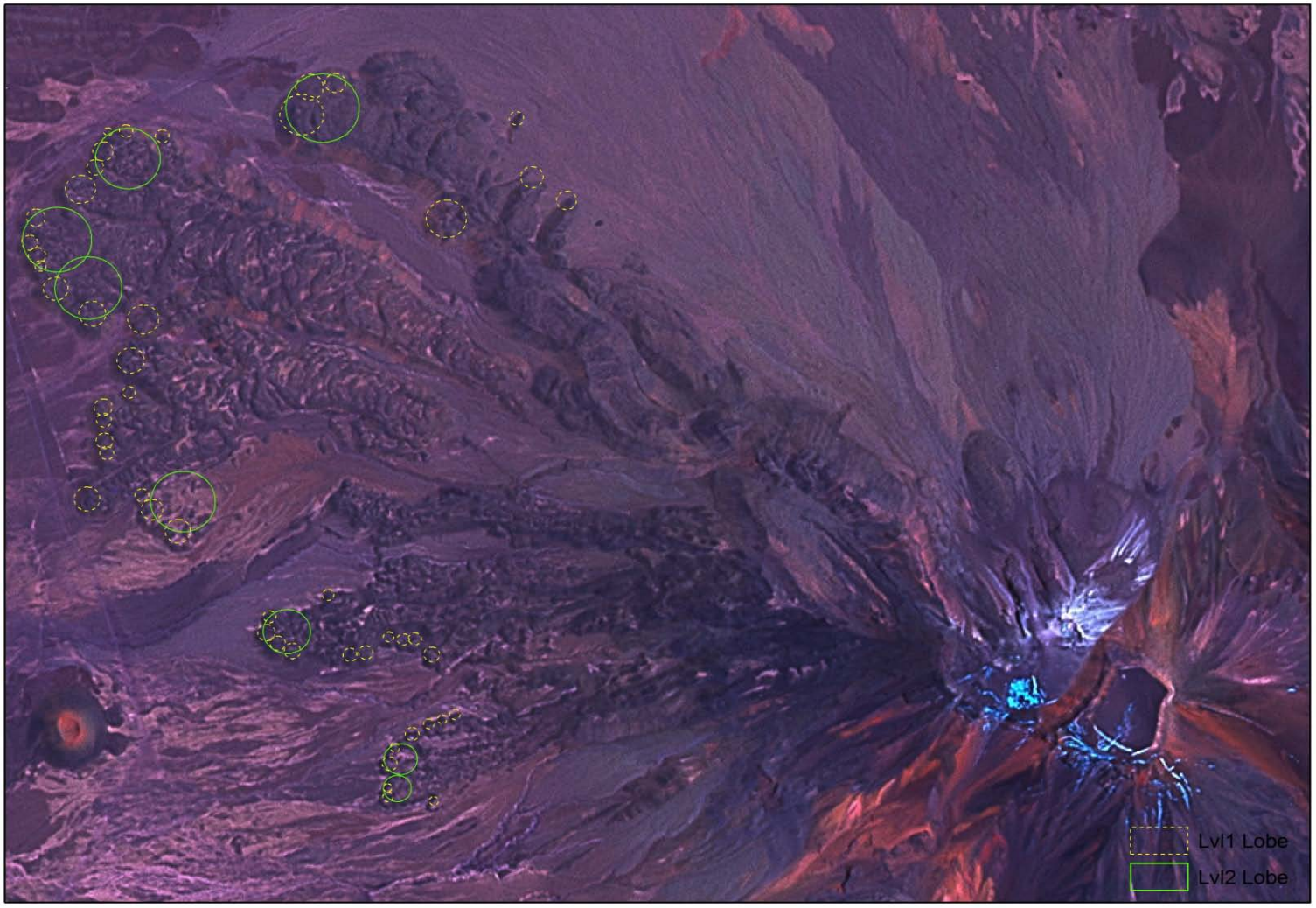

San Pedro Lava Lobes
SAD_1969_Lambert_Conformal_Conic
(62.7%) O'Callaghan & Francis, 1986

Shasta

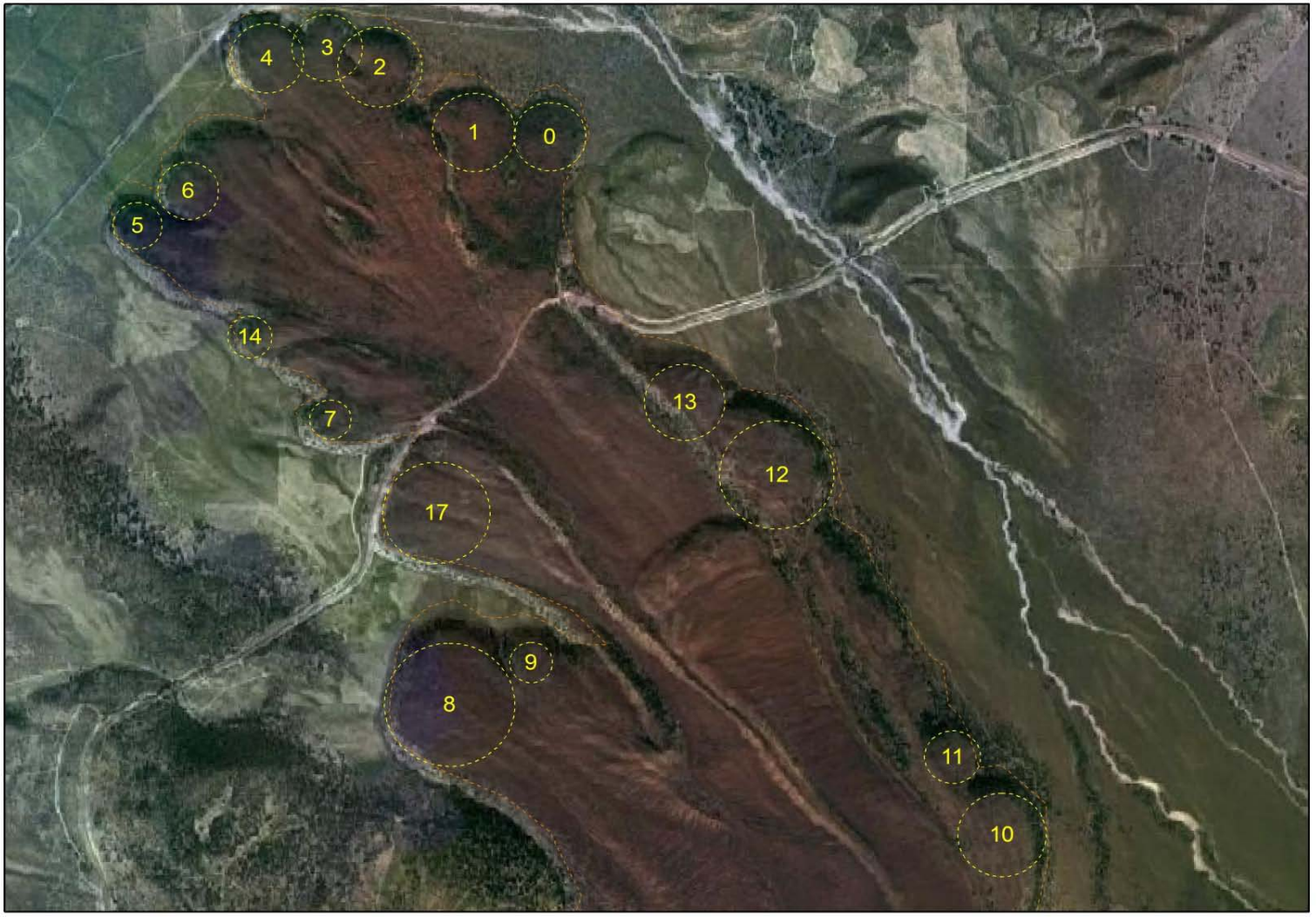

Shasta Lava Lobes
NAD_1983_UTM_Zone_10N
(62%) Miller, 1980

Socompa

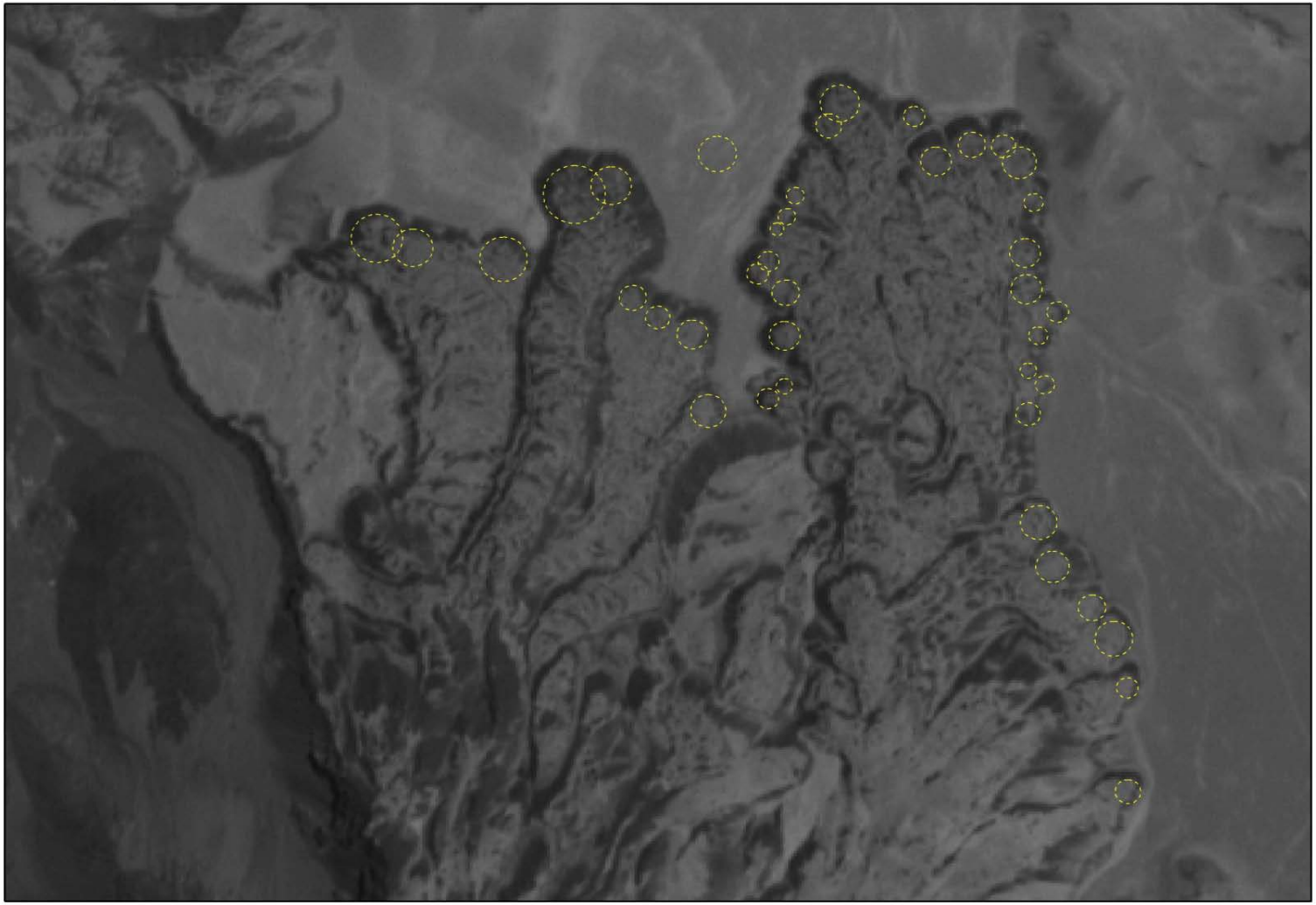

Socompa North Lava Lobes
SAD_1969_Lambert_Conformal_Conic
(63%) Ramirez, 1988

N

1,000 Meters

SP Flow

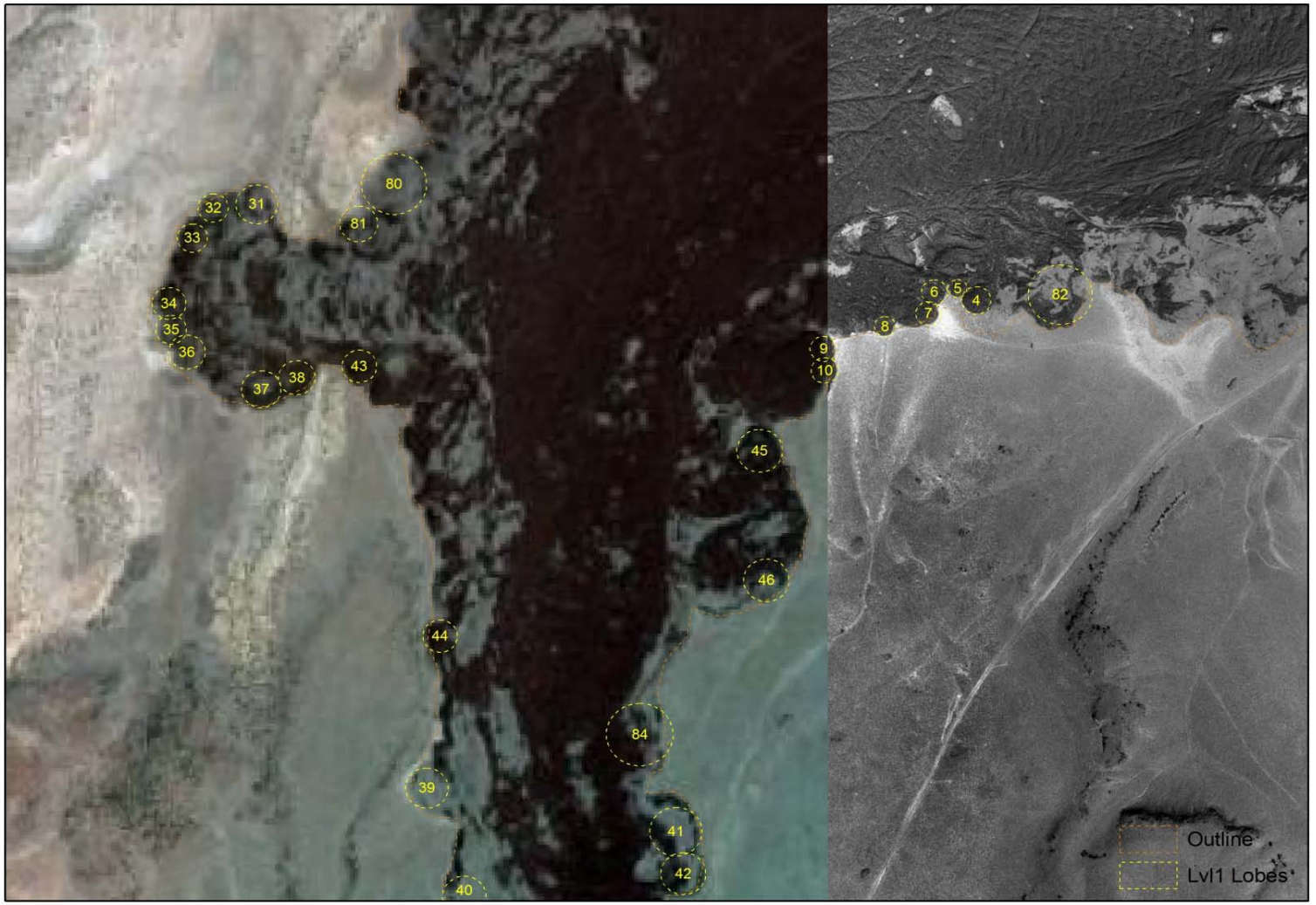

SP Flow
NAD_1983_UTM_Zone_12N
(58.5%) Schahrer et.al, 1980

1,000 Meters